Evidence that crater flux transfer events are initial stages of typical flux transfer events

H. Zhang,[1] M. G. Kivelson,[1] K. K. Khurana,[1] J. McFadden,[2] R. J. Walker,[1] V. Angelopoulos,[1] J. M. Weygand,[1] T. Phan,[2] D. Larson,[2] K. H. Glassmeier,[3,4] and H. U. Auster[3]

Received 22 October 2009; revised 23 March 2010; accepted 30 March 2010; published 28 August 2010.

[1] Bipolar magnetic perturbations along the normal to the local magnetopause associated with field magnitude enhancements are signatures of typical flux transfer events (T-FTEs) and are interpreted as evidence of encounters with magnetic flux ropes with strong core fields. If the field magnitude dips at the center of the signature, we identify the event as a crater FTE (C-FTE). In the multiple-spacecraft data of the Time History of Events and Macroscale Interactions During Substorms (THEMIS) between 1 May and 31 October 2007, we have identified 622 FTEs of which only 23 manifested C-FTE signatures. We analyze a C-FTE (30 July 2007) that evolved into a T-FTE and compare its properties with those of a T-FTE (May 20, 2007). For all 23 C-FTEs and 35 confirmed T-FTEs, we compare solar wind conditions and internal plasma and field properties. The similarity of solar wind properties for events in the two classes suggests that differences in their structures are not related to the solar wind conditions. Systematic differences in internal peak fields ($B_{\text{C-FTE}} < B_{\text{Magnetosphere}} < B_{\text{T-FTE}}$) and averaged number densities ($N_{\text{T-FTE}} < 0.5 \times N_{\text{Magnetosheath}} < N_{\text{C-FTE}}$) between the two groups are consistent with the evolution of C-FTEs into T-FTEs. We propose that parallel flows inside C-FTEs deplete the internal ion densities and reduce the thermal pressures as the central field magnitude increases to maintain pressure balance.

Citation: Zhang, H., et al. (2010), Evidence that crater flux transfer events are initial stages of typical flux transfer events, *J. Geophys. Res.*, *115*, A08229, doi:10.1029/2009JA015013.

1. Introduction

[2] Magnetic reconnection on the dayside magnetopause was first proposed by *Dungey* [1961] as a fundamental process for solar wind–magnetosphere coupling. Magnetic connection allows exchange of mass, momentum, and energy between these two regions. Acceleration, deceleration, or deviation of flows on the magnetopause relative to the background sheath flow are often used to identify reconnection [*Paschmann et al.*, 1979; *Sonnerup et al.*, 1981; *Gosling et al.*, 1990; *Scurry et al.*, 1994; *Pu et al.*, 2007]. A characteristic magnetic field signature consisting of a transient bipolar variation of the component along the normal to the local magnetopause, typically associated with enhancements in field strength, is also interpreted as evidence of reconnection [*Russell and Elphic*, 1978]. The coexistence of sheath and magnetospheric particles within these magnetic signatures implies magnetic connection between the sheath and magnetosphere and strongly supports the reconnection picture [*Thomsen et al.*, 1987]. These transient reconnection-associated magnetic signatures are referred to as flux transfer events (FTEs) [*Russell and Elphic*, 1978]. In some FTE cases, the field magnitude increase shows a crater-like dimple in the center and is referred to as a "crater FTE" (C-FTE) [e.g., *LaBelle et al.*, 1987; *Farrugia et al.*, 1988]. The phenomenological definitions of the different forms of FTEs characterize a distinct physical entity: a flux rope. A typical FTE (T-FTE) is a flux rope in which the field in the core region is compressed by the curvature force of surrounding twisted fields [e.g., *Paschmann et al.*, 1982; *Hasegawa et al.*, 2006]. In a C-FTE, enhanced plasma pressure at the core of the flux rope (outward thermal pressure gradient force) supplements the magnetic pressure in counteracting the inward forces arising from the surrounding twisted fields. The reduced magnetic pressure at the center of the structure may lead to a local minimum of field magnitude [e.g., *Ding et al.*, 1991; *Sibeck et al.*, 2008].

[3] It has been suggested that the structure of an FTE on the magnetopause depends on the interplanetary magnetic field (IMF) conditions under which magnetic reconnection

[1]Institute of Geophysics and Planetary Physics, University of California, Los Angeles, California, USA.
[2]Space Sciences Laboratory, University of California, Berkeley, California, USA.
[3]Institut für Geophysik und Extraterrestrische Physik, TUBS, Braunschweig, Germany.
[4]Max Planck Institute for Solar System Research, Katlenburg-Lindau, Germany.

0148-0227/10/2009JA015013

occurs. It is firmly established that reconnection can occur on the low-latitude dayside magnetopause for a wide range of the local magnetic clock angles [e.g., *Paschmann et al.*, 1986; *Gosling et al.*, 1990; *Scurry et al.*, 1994; *Phan et al.*, 1996]. "Antiparallel reconnection" or "quasi-antiparallel reconnection" occurs when the two interacting regions have nearly antiparallel magnetic fields [*Crooker*, 1979]. *Ding et al.* [1991] have proposed that a C-FTE with a weak core field forms in the presence of antiparallel reconnection because of the absence of a strong guide field. "Component reconnection" takes place if the shear angle is not large, as for example, when the IMF has a large B_Y component or even tilts somewhat northward [*Gonzalez and Mozer*, 1974; *Sonnerup*, 1974; *Cowley*, 1976]. In that circumstance, it has been suggested that the strong guide field contributes to the formation of a strong core field, producing a T-FTE [e.g., *Lee and Fu*, 1985; *Scholer*, 1988].

[4] We test the relation between the type of FTE observed and the IMF clock angle. Our statistical analyses do not reveal a correlation. On the other hand, we find both through statistical analysis and a case study that there are systematic differences between the two types of structures. Our analyses presented in the following sections lead us to propose that FTEs initially form as C-FTEs and evolve into T-FTEs with a reduction of central plasma pressure resulting from transport of plasma along their axes.

[5] Critical to establishing the difference between C-FTEs and T-FTEs is the need to remove ambiguous events from the data set analyzed. The signatures of a C-FTE identified in single spacecraft data can be mimicked when a short-duration pressure pulse moving along the magnetopause displaces the magnetopause into the magnetosphere. As the displaced magnetosheath moves over an observing spacecraft, changes of the normal component of the field and a field magnitude perturbation with a central minimum may be interpreted as a C-FTE. In this picture, a C-FTE signature could be produced in the absence of magnetic reconnection [*Sibeck*, 1990, 1992; *Sibeck and Smith*, 1992]. Even a typical FTE in which the total pressure is maximum at the center can mimic the signature of a C-FTE on the magnetopause (see data presented by *Sibeck et al.* [2008] and *Zhang et al.* [2008]). On the other hand, a C-FTE can be taken for a typical one if it is identified in data from a single spacecraft that does not go through the FTE's central weak field region and just grazes the outer layers, where the field magnitude exceeds that of the ambient background. Such a grazing trajectory will register a central peak in field magnitude associated with bipolar perturbations. Therefore, data from spacecraft trajectories that cross an FTE with small impact parameter are required for unambiguous identification of the FTE structure. A multispacecraft mission increases the probability that one spacecraft will cross close to the central region of an FTE. Fortunately, the required measurements were obtained by the multispacecraft Time History of Events and Macroscale Interactions During Substorms (THEMIS) mission during its first year of operation. In the initial stage, the five spacecraft moved in a "pearls-on-a-string" configuration almost on the same orbit, which for many months typically crossed the magnetopause twice per orbit, inbound and outbound, respectively [*Angelopoulos*, 2008]. Near the magnetopause, the spacecraft were distributed linearly with several hundred kilometers to several Earth-radii separations along the magnetopause normal direction, thus, providing unique opportunities to investigate FTEs with high spatial resolution.

[6] In section 2, we briefly introduce the instrumentation and our working definitions for FTEs. On the basis of our working definitions, we identified 622 FTEs in the time interval examined, among which only 23 events were confirmed to be C-FTEs. In section 3, we briefly introduce a flux rope model modified from one initially proposed by *Kivelson and Khurana* [1995]. The modified model can describe both T-FTEs and C-FTEs. In section 4 we report two case studies and try to fit them to our model. Section 5 presents some statistical studies that reveal systematic differences in the internal plasma and magnetic field properties found in these two types of FTEs but finds little difference in their associated solar wind conditions. The suggestion that a C-FTE is an early stage of a T-FTE and that the external solar wind conditions such as the IMF clock angles and the sheath ion beta do not dictate the form of an FTE is proposed on the basis of these comparisons. Our study is discussed and summarized in section 6.

2. Instrumentation and Event Selection

[7] All the FTEs studied in the present paper were recorded by the instruments on board the five THEMIS spacecraft: the electrostatic analyzers, the solid state telescopes (SST), and the fluxgate magnetometers (FGM). The technical details of these instruments are provided by *Angelopoulos* [2008], *McFadden et al.* [2008], and *Auster et al.* [2008]. Plasma and field data presented in this paper are generally at 3 s resolution. The magnetic field data fitted to the flux rope model are used at the higher temporal resolution of 0.25 s. Vector data are shown in the Geocentric Solar Magnetospheric (GSM) coordinate system or, where appropriate, in the magnetopause local coordinate system (LMN), in which $\vec{N}$ points outward along the normal to the magnetopause determined from an empirical magnetopause model [*Shue et al.*, 1998; *Wang et al.*, 2005], $\vec{M}$ is determined by $\vec{Z}_{\mathrm{GSM}} \times \vec{N}$, and $\vec{L}$ completes the right-hand orthogonal system through $\vec{N} \times \vec{M}$. We did not align any principal axis of this local magnetopause coordinate system LMN along the axes of FTEs because of the significant uncertainty in determining FTE orientations.

[8] The THEMIS data used in this paper were acquired between 1 May and 31 October 2007. Initially, all five spacecraft were lined up in almost the same orbit with an apogee of 15.4 R_E. Near the magnetopause, the maximum separation among spacecraft along the magnetopause normal direction was several Earth radii. After 15 September, the apogees of P1 and P2 were changed to 30 and 20 R_E, P3 and P4 to 12 R_E, and P5 to 10 R_E [*Angelopoulos*, 2008]. On these orbits, the spacecraft still crossed the magnetopause but at significantly different times and with separations basically along the magnetopause rather than along the normal direction. Figure 1a shows the typical orbits of THEMIS in May, July, and October. Since THEMIS is an equatorial-orbit spacecraft mission, all the orbits are shown only in the equatorial plane of the GSM coordinate system. With spacecraft separated along the magnetopause normal, an FTE can be occasionally encountered by all five probes. In most cases, only some of the spacecraft cross the FTE and

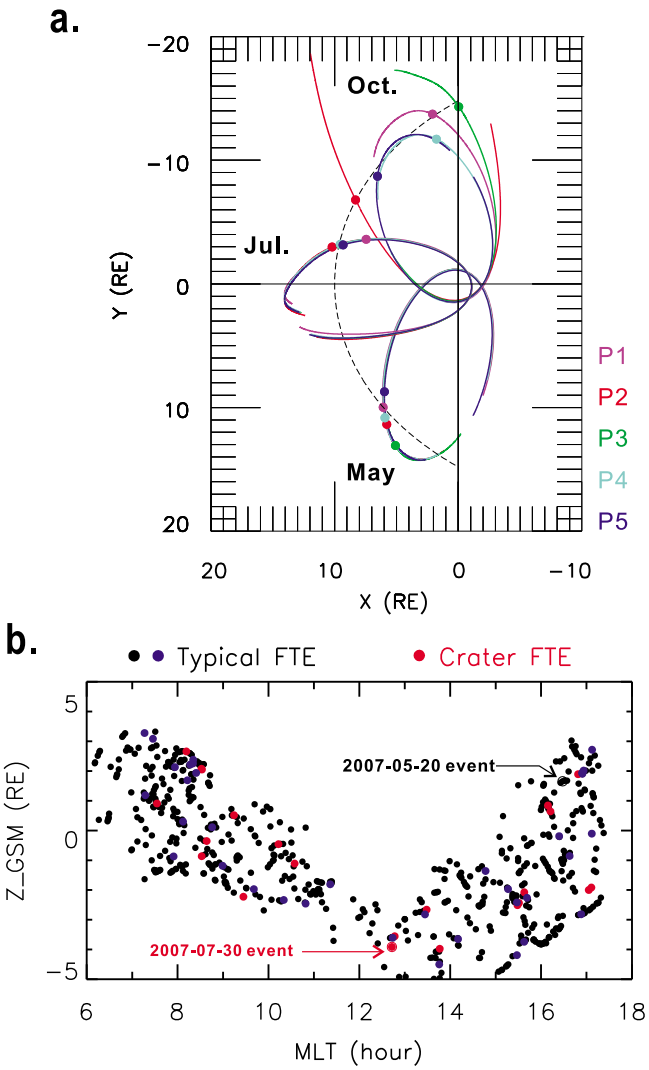

Figure 1. (a) Typical THEMIS orbits in May, July, and October 2007 projected on the GSM X-Y plane. The dashed curve is a modeled magnetopause. Different colors denote the five spacecrafts. (b) The observed positions of 23 C-FTEs (red dots) and 599 T-FTE-like events (blue and black dots) are shown in a Z_{GSM} versus magnetic local time plot. Thirty-five confirmed T-FTEs indicated by the blue dots form the subset used to compare with the 23 C-FTEs.

the rest remain in the magnetosheath or in the magnetosphere. We can determine the background sheath or magnetospheric conditions using data from probes located in the sheath or in the magnetosphere either before or after their FTE encounters or during intervals when other probes were encountering an FTE.

[9] Following *Russell and Elphic* [1978], a transient bipolar variation of the normal component of the magnetic field on the magnetopause, associated with enhancements in field magnitude, is identified as an FTE in this paper. An enhancement of the total pressure is also used as a criterion for event selection as suggested by *Paschmann et al.* [1982]. Events with wave-like continuous magnetic fluctuations (two or more cycles) are not identified as FTEs because they are likely to be surface waves on the magnetopause [e.g., *Sibeck et al.*, 1989]. We could have missed many short timescale bipolar perturbations as FTEs (10 s or shorter), but we have obtained many representative events. If the field magnitude increase shows a crater-like dimple in the center, the event is referred to as a "C-FTE" [e.g., *LaBelle et al.*, 1987; *Farrugia et al.*, 1988], whereas if the associated field strength increase shows just one peak, we cannot label it as a "T-FTE" unless we can establish that the impact parameter of the observing spacecraft was sufficiently small. Later in the paper we undertake a statistical analysis of plasma and field properties of the two types of FTEs. For those statistical studies, we include the events only if the observing spacecraft has entered the actual flux rope region. This restriction excludes events in which the observations could have been produced by a pressure pulse in the solar wind. Because of the possibility of misidentifying a C-FTE as T-FTE, we have applied the minimum variance analysis (MVA) technique and another method, described in detail in section 5, to confirm our event classification. From 1 May to 31 October 2007, we found only 23 C-FTEs but 599 events with T-FTE-like signatures. Figure 1b shows the distribution of their observed locations in a plot of magnetic local time versus Z_{GSM}. The C-FTEs are plotted as red dots, and the events with typical FTE signatures are plotted in black dots. A subset of 35 events with typical FTE signatures, which are confirmed to be T-FTEs by the MVA technique and used in comparisons with C-FTEs, is plotted as blue dots. The dawn-dusk asymmetry of the locations of the FTEs is caused by the dawn-dusk asymmetry of the orbits of THEMIS.

[10] When we surveyed all the events, we found that those we have designated as T-FTEs produce four different types of magnetic perturbations that we believe relate to impact parameters of the trajectories of the spacecraft relative to the FTE. In Figure 2, we show these four types of magnetic signatures. Bipolar magnetic perturbations in the normal direction to the local magnetopause, B_N, are required for all the cases, but the field strength (B_T) profiles depend on the trajectory. On the trajectory skimming the FTE on the magnetosheath side and labeled T1 in Figure 2, B_T shows a single strong peak symmetric about the center of the bipolar B_N; the asymptotic B_T has magnetosheath field properties, i.e., is small compared with the magnetospheric field nearby and fluctuates significantly (Figure 2a). On trajectory T2, a spacecraft also records a single peak in B_T centered at the reversal of B_N, but that peak is bounded by two dips; the asymptotic B_T has magnetospheric field properties, i.e., is strong and steady (Figure 2b). On trajectory T3, the field magnitude B_T increases as the magnitude of B_N begins to grow, but dips at the center of the bipolar B_N; again the signature asymptotes to the magnetospheric field (Figure 2c). On trajectory T4, the perturbations have a structure similar to that described for T1, but the field asymptotes to a strong and steady magnetospheric field (Figure 2d). For C-FTEs, the signatures are basically the same as T-FTEs, but, on trajectories that come close to the center of the structure (T2 and possibly T1), B_T has a dip within the central peak (not shown in Figure 2). The schematic of Figure 2e shows our interpretation of the configuration near the magnetopause and how the structure relates to the signatures described on the different trajectories. Only T1 and T2 actually go through FTE structure, and T3 and T4 pass by the structure (ellipse in Figure 2e). As suggested by *Zhang et al.* [2008], the

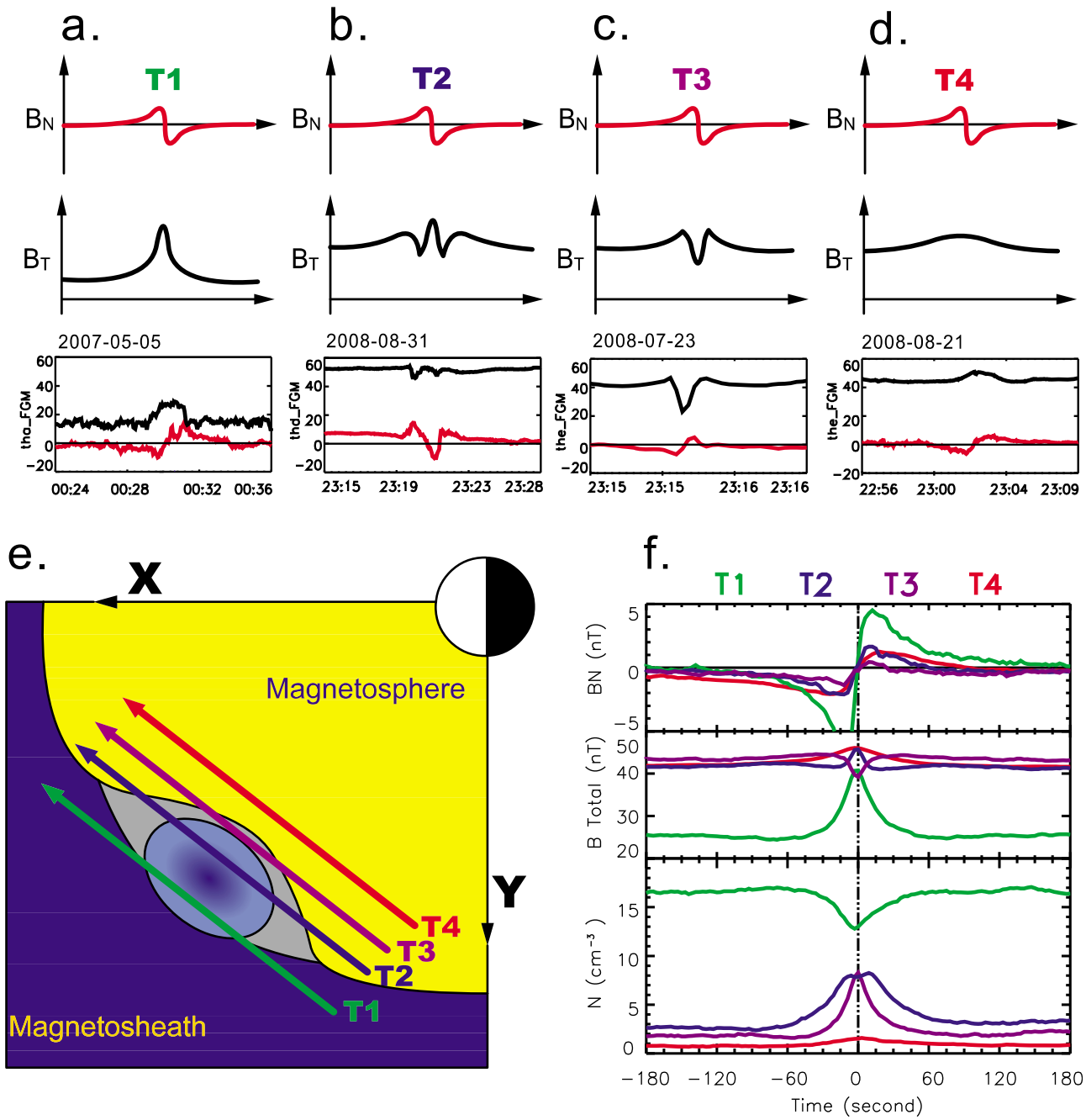

Figure 2. The distinct signatures from different trajectories relative to an FTE. (a–d) Typical perturbations in B_N (red) and B_T (black) on trajectories T1, T2, T3, and T4. The top two frames show schematically the typical signatures, and the bottom frames show data from actual events as examples. (e) The configuration of the plasma layers near the magnetopause and four trajectories with different impact parameters: T1, T2, T3, and T4. The plane shown is perpendicular to the axis of an FTE (ellipse area), and the FTE is embedded within an expanded and distorted magnetopause current layer within which the field magnitude is weak (gray region) corresponding to the field strength dips on T2 and T3. Blue and yellow represent the magnetosheath and the magnetosphere, respectively. (f) Plots of the superposed epoch analyses of B_N, B_T, and N (number density) for all events on the four trajectories. The time interval is 6 min, and the reference time corresponds to the zero-crossing of B_N. The color coding (green for T1, blue for T2, purple for T3, and red for T4) corresponds to that used in Figure 2e. The averaged B_N and B_T reproduce the expected properties of the four trajectories as shown in Figures 2a, 2b, 2c, and 2d.

FTE structure is embedded within an expanded and distorted magnetopause current layer (the gray region in Figure 2e) within which the field magnitude is weak (dips in B_T on T2 and T3).

[11] Distinct patterns of density changes correspond to the different patterns of magnetic perturbations used to identify the spacecraft trajectories T1–T4 and support the model of Figure 2e. Figure 2f shows the superposed epoch analyses (relative to the reversal time of the B_N perturbation) of B_N, B_T, and N (number density) within ±3 min for all events on the four trajectories. As expected, the averaged B_N and B_T show the signatures that we used in classifying the measurements into subgroups T1–T4. Plasma density (bottom panel of Figure 2f) was not used in the classification but on average displays changes consistent with the interpretation illustrated in Figure 2e. On average for passes T1, the plasma perturbation emerges from a dense plasma background (N is over 15 cm^{-3}), consistent with magnetosheath properties, while on passes T4, it emerges from a plasma with density as low as 1 cm^{-3}, consistent with magnetospheric plasma. On T2 and T3, the background number densities (2–3 cm^{-3}) are between those on the previous two trajectories, suggesting that these trajectories passed through the low latitude boundary layer before and after encounter with the FTEs.

[12] The number densities decrease on T1 and increase on T2 and T3 during the time when the spacecraft is thought to be located in the gray region or within the FTE (Figure 2e). In these regions, the number densities fall between the background sheath number density (over 15 cm^{-3}) and the background density in the low latitude boundary layer (below 3 cm^{-3}), consistent with formation of the flux rope by reconnection. On T4, the number density also increases reaching a level close to the background level on T3. This correspondence can be understood if the motion of the FTE along the magnetopause brings the boundary closer to the path, T4, thereby, moving the low-latitude boundary layer over the spacecraft. The picture inferred from the averaged number density along each class of trajectory is consistent with that inferred from the magnetic signatures.

[13] In seeking to exclude from our database signatures that mimic FTEs, in addition to eliminating continuous wave-like magnetic fluctuations, we must also exclude events caused by pressure pulses in the solar wind, as discussed above. Pressure pulses produce indentations of the local magnetopause and can generate bipolar magnetic perturbations in the direction normal to the local magnetopause [*Sibeck et al.*, 1989]. We must consider whether the increases of B_T identified in the schematics of Figures 2a–2d can be produced by pressure pulses. The field magnitude within the flux rope is comparable to and may be even stronger than the magnetospheric field strength (T1 and T2). These observations cannot be understood in the context of magnetopause indentations caused by pressure pulses, which can produce perturbations with a bipolar B_N signature but have B_T a minimum at the center of the bipolar signature, as proposed by, for example, by *Sibeck* [1992]. While on T3 and T4, the perturbations can be produced by pressure pulses [*Sanny et al.*, 1996].

[14] Because a pressure pulse can mimic an FTE observed on trajectories such as T3 and T4 that do not penetrate the actual structure [*Sanny et al.*, 1996], we focus on cases for which the signatures are those that we have associated with trajectories of type T1 or T2. In particular, in our statistical studies of the plasma and magnetic field properties within FTEs, we used data only from cases of type T1 and T2 that are thought to cross the actual FTE structure. Some of the 622 events with signatures of types T3 and T4 may have been produced by surface waves or pressure pulses, but they are not included in the statistical database that is used to distinguish properties of T-FTEs from C-FTEs.

3. A model for Flux Ropes in Equilibrium

[15] Since we have multispacecraft measurements through and around FTEs, if we assume that FTEs are in steady state, a useful approach to the interpretation of FTE structure is to fit the measurements to a quantitative model. A number of parameterized flux rope models have been proposed. Some of them simply assume that flux ropes have circular cross sections and ignore the ambient field (e.g., the force-free model by *Lundquist* [1950] and the non-force-free model by *Elphic and Russell* [1983]); *Moldwin and Hughes* [1991] noticed the asymmetry of flux ropes' cross sections and modified the circular-cross-section model by embedding a flux rope in an external sheared field to generate the asymmetry, thereby, adopting a model closer to the actual situation. In this paper we slightly modified and applied a model of flux rope embedded within a Harris current sheet, which was first introduced by *Kivelson and Khurana* [1995]. The magnetic fields both inside and outside a flux rope can be described self-consistently for appropriate boundary configurations, and the magnetic structure can be force-free or non-force-free depending on the selected pressure solution. Hereafter in the paper, this model is referred to as KK95 model.

[16] Assuming that the current density $\vec{j}$ depends exponentially on the magnetic vector potential **A**, *Kivelson and Khurana* [1995] found a solution of equation (1) that describes flux ropes in a 2-D system

$$\nabla^2 A = -\mu_0 j = -\exp(A), \tag{1}$$

where the scalars A and j are the components of **A** and **j**, respectively, along the axis of the flux rope.

[17] This model has been successfully applied to the analyses of flux ropes embedded within a transition region that is actually an expanded and distorted magnetopause current layer on the dayside magnetopause [*Zhang et al.*, 2008] and of flux ropes embedded within the current sheet in the magnetotail [*Kivelson and Khurana*, 1995]. Kivelson and Khurana also developed a model that can describe the thermal pressure P within a flux rope. In this paper in order to describe C-FTEs, we modify their solution and write the pressure in the form

$$P = P_* + \frac{P_o}{\chi^2} e^{-\gamma\varepsilon/\chi^{\kappa-2}}, \tag{2}$$

where ε is a free parameter related to the shape of flux rope's cross section; when $\varepsilon \to 0$, the field solution reduces to a Harris neutral sheet field, and as ε increases, the cross section becomes less oblate and more circular in shape; γ and κ are fit parameters modulating the pressure profile through the cross section; and χ is a function of position (x_1, x_2): $\chi = (1+\varepsilon^2)^{1/2} \cos h(x_1/L) + \varepsilon \cos(x_2/L)$, here L is the scale length

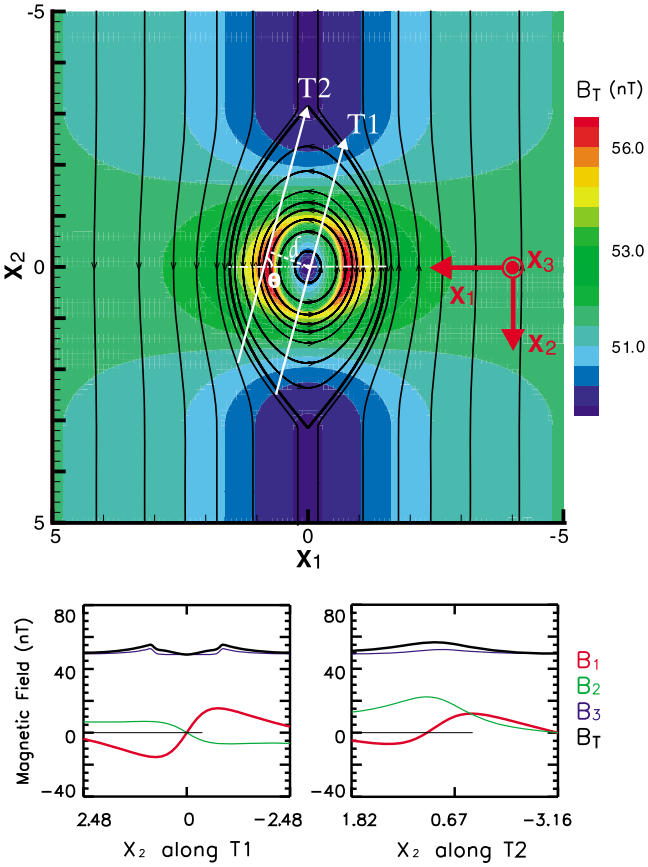

Figure 3. The upper plot shows a cross-sectional map of a modeled C-FTE embedded in a Harris current sheet. The colored contours denote the magnetic field strength; the black curves show some representative magnetic field line projections onto this plane. The white straight lines show two possible trajectories across the flux rope structure; the lines are defined by two parameters: d is the distance from the center of the flux rope to the trajectory projection (impact parameter), and θ is the angle between the trajectory and the short axis of the oval cross section. The lower two frames show the model magnetic fields along the two trajectories in the upper plot. The trajectory T1 registers a C-FTE signature, while T2 registers a T-FTE signature.

and (x_1, x_2) are orthogonal coordinates transverse to the flux rope axis.

[18] In this solution, the first term, P_*, is a uniform background thermal pressure, which does not contribute to the pressure balance; $P_* + P_o$ is the pressure at the center of the current sheet when $\varepsilon \to 0$ and pressure balance across the system gives P_o in terms of the magnetic pressure at large $|x_1|$. The second term $\frac{P_o}{\chi^2}e^{-\gamma\varepsilon/\chi^{\kappa-2}}$ represents the pressure variation through the cross section of the FTE. When $P_o = 0$, the thermal pressure P is uniform and does not contribute to the force balance, and thus, the structure is electromagnetically force-free; when $P_o \neq 0$, the flux rope is referred to as non-force-free. The equation represents a T-FTE for positive κ and for weakly negative κ (precise values depend on ε and γ, but the equation can represent a C-FTE for sufficiently negative κ, in which case, P increases rapidly toward the FTE's center. This solution satisfies all the constraints proposed by *Kivelson and Khurana* [1995], although they chose $\frac{P_o}{\chi^2}(1 - \gamma\varepsilon/\chi^{\kappa-2})$ as their solution, which is actually the first two terms of the Taylor series of equation (2) and can only describe flux ropes with strong core fields (T-FTEs).

[19] We adopt the coordinate system ($\mathbf{x}_1$, $\mathbf{x}_2$, $\mathbf{x}_3$) used by *Zhang et al.* [2008], in which $\mathbf{x}_1$ is perpendicular to the current sheet in which the flux rope is embedded; and $\mathbf{x}_2$ and $\mathbf{x}_3$ are parallel to the current sheet with $\mathbf{x}_3$ along the axis of the flux rope and $\mathbf{x}_2$ perpendicular to the axis (see Figure 3). In this coordinate system, the corresponding magnetic field is given as:

$$\begin{bmatrix} B_1 \\ B_2 \\ B_3 \end{bmatrix} = \begin{bmatrix} B_{2,\infty}\varepsilon \sin((x_2+\pi)/L)/\chi \\ B_{2,\infty}(1+\varepsilon^2)^{1/2}\sinh(x_1/L)/\chi \\ (B_{3,\infty}^2 + B_{2,\infty}^2/\chi^2 - 2\mu P_o e^{-\gamma\varepsilon/\chi^{\kappa-2}}/\chi^2)^{1/2} \end{bmatrix}, \quad (3)$$

where $B_{2,\infty}$ and $B_{3,\infty}$ are the asymptotic values of B_2 and B_3 at $x_1 \to +\infty$; the other free parameters are the same as in equation (2). It is clear that six free parameters ε, γ, κ, L, $B_{2,\infty}$, and $B_{3,\infty}$ control the form of the structure. When $\varepsilon \to 0$, pressure balance within the current sheet requires $P_o = B_{2,\infty}^2/2\mu_0$. We notice that the solutions for the two azimuthal components, B_1 and B_2, are independent of the thermal pressure, whereas the core field, B_3, depends on it. This model is a 2-D model, and no parameter changes with x_3. The model can apply to a periodic array of flux ropes but also can be linked to a Harris neutral sheet field at the boundary of a single unit of the periodic array, and in this paper we adopt the latter form. That is to say, within the region of $|x_2| \leq \pi$, we adopt a solution of the equation (2) with a nonzero ε describing a single flux rope structure, while outside that region ($|x_2| > \pi$), we apply the same solution but with $\varepsilon = 0$, which describes a Harris neutral sheet; these two solutions are consistently joint at $|x_2| = \pi$.

[20] We present a C-FTE example described by the KK95 model in Figure 3; in this case, $B_{2,\infty} = 16$ nT, $B_{3,\infty} = 49$ nT, $\varepsilon = 1.0$, and $\kappa = -16$. The upper plot shows a map of the cross section of the flux rope. The color contours indicate the field magnitude through the cross section, and the black curves show the projections of the field lines onto the cross-section plane. The coordinate axes are given in units of L, the scale length. On the basis of our working definition, the flux rope is a C-FTE because the field strength in the core region is weaker than that in the outer layers. We can characterize possible magnetic signatures of this structure by selecting different trajectories. Because the KK95 model is 2-D and any motion of spacecraft along the axis of the flux rope will not change the magnetic signatures, we need only 2 parameters to define a trajectory: d is the distance from the center of the flux rope to the projection of the trajectory on the cross-section plane (impact parameter), and θ is the angle between the trajectory projection and the short axis of the flux rope ($-\mathbf{x}_1$). When we set $\theta = 75°$ and $d = 0$, the trajectory T1 goes right through the center of the flux rope, and we detect C-FTE signatures: a bipolar B_1 structure and an enhancement in field magnitude with a central depletion (the bottom left plot in Figure 3). Actually, all the trajectories going through the field depletion region (the green and blue region in the center of the flux rope) will produce C-FTE signatures, but not all trajectories will do so even though the structure is a C-FTE. For example, when $\theta = 75°$ and $d = 0.85$ (trajectory T2 in the

upper plot of Figure 3), the KK95 model produces T-FTE-like signatures: a bipolar B_1 associated with an enhancement in field magnitude (the bottom right plot in Figure 3). From this test, we learn that we cannot tell whether or not an FTE is a T-FTE unless we know the impact parameter of spacecraft trajectory.

4. Case Studies

[21] In this section we present one C-FTE event, which was evolving with time, and one T-FTE event, which was approximately in steady state. We compare their internal plasma and field behaviors, and we also try to fit them to the KK95 equilibrium flux rope model.

4.1. A C-FTE on 30 July 2007

[22] At about 1424 UT on 30 July 2007, a C-FTE was recorded by THEMIS near the noon meridian and 4 R_E below the subsolar point (Figures 1b and 4a) when all five spacecraft were orbiting inbound in a pearls-on-a-string configuration. The spacecraft separations were basically along the normal to the magnetopause, P1 was the innermost probe, followed by P2, P3, P4, and P5 (Figures 4a and 4b).

[23] Figure 4c presents an overview of the magnetic field data from all five probes displayed in the LMN coordinate system previously defined. The frames, from top to bottom, are ordered by the radial distance of the spacecraft from outermost to innermost. It is worth noting that the normal components B_N well away from the FTE signatures are very small, indicating that the coordinate system LMN has been well chosen. During the time interval shown, P5 was immersed in the magnetosheath and detected a disturbed background sheath magnetic field whose magnitude was 20 nT. The dominant component was in the **M** direction, initially pointing duskward but turning to dawn after 1433 UT. Around 1424 UT, P4, P3, and P2 encountered the FTE, and all of them detected clear bipolar structures in their normal components, associated with enhancements in field strength (marked by the vertical dash lines in Figure 4c). The axis of the FTE is hard to determine precisely, but the best fit of the observations to the KK95 model gave an orientation not far from the L direction (see section 4.1 for details). The azimuthal field of the helical structure would then have been approximately in an N-M plane. At P4, the dominant azimuthal field was in the M direction, implying that P4 grazed the sheathside edge of the FTE. P3 and P2 crossed the FTE at small-impact parameters where the azimuthal components were mainly in the normal direction; both of them probably crossed close to the center of the FTE and observed dips in field magnitude at the center of the bipolar signatures. P1 remained in the magnetosphere and a bit duskward of the other probes; it remotely sensed the magnetic perturbations, a bipolar signature, and a small enhancement of field, with a delay of 1 min (1425 UT). In the magnetosphere, the field strength was more than 40 nT, with the dominant component in the L direction and a small negative component in the M direction. The magnetic field observations in the magnetosheath and in the magnetosphere allow us to calculate the IMF clock angle of about 90°. These external fields on the two sides of this FTE are neither equal nor antiparallel as in a Harris current sheet.

[24] On the basis of the magnetic field data as well as the plasma data, a diagram is given in Figure 4b to show the approximate trajectories of the five spacecraft relative to the FTE. Before and after observing the FTE signatures, from 1415 to 1424 UT and from 1425:30 to 1435 UT, respectively, P3 and P2 were located in the magnetosphere where the field magnitude was over 40 nT. These two probes moved initially from the magnetosphere to the central region of the FTE and then back to the magnetosphere; the probe P4, which grazed the magnetosheath side of the FTE (B_M was positive), also entered the magnetosphere after crossing the FTE, suggesting that the inner edge of the local magnetopause was displaced deep into the magnetosphere and that the FTE was embedded within an indentation, as shown in Figure 4b. Dips in the field strength were observed on both sides of the FTE at P2 and P3 as well as at P4. The distinct plasma properties in these field strength dips, which will be shown later in this section, suggest that these field-strength dips give evidence of passage through a region distinct from the FTE, the low-latitude boundary layer, the magnetosphere, and the magnetosheath [*Sibeck et al.*, 2008]. This region is an expanded magnetopause current layer that *Zhang et al.* [2008] called a "transition region"; in this paper we use the same term. P2 and P3 observed the transition region both ahead of and behind the FTE structure. On those trajectories, B_N was the dominant azimuthal component and B_M was small but negative. On the P4 trajectory, P4 encountered the transition region on the magnetosheath side of the FTE. B_M was the dominant azimuthal component and it was positive. The field in the transition region had the same sense of rotation as the field within the FTE structure. The transition region probably envelopes the FTE structure as shown in Figure 4b, although we have no probe in the transition region on the magnetospheric side of the FTE to confirm this expectation. However, we do find the transition region on both magnetosheath and magnetospheric sides of the event of 20 May 2007 for which we do have probes on both sides. Field discontinuities existed on the boundaries between the transition region and the FTE and between the transition region and the magnetosphere (or the low latitude boundary layer). This can be seen in Figure 4c, as well as in the high-resolution magnetic field data at P2 and P3 in Figure 6. The field discontinuities on the boundaries suggest that the axis of the FTE must have rotated as it moved along the dayside magnetopause. Enhanced electric currents present on the boundary of the FTE are evidently associated with the sheared fields on the boundaries. The distinct plasma properties within the transition region will be discussed below.

[25] The inferred trajectories of the spacecraft through the FTE and its surroundings were confirmed by the plasma data. Figure 5 shows the plasma data as well as the magnetic field data from P2 between 1423 and 1427 UT. At the top of the plot, the numbers denote different regions near the magnetopause: "0" stands for the magnetosphere, "1" stands for the low-latitude boundary layer (LLBL), "2" stands for the transition region between FTE and LLBL, and "3" stands for the FTE (the numbers correspond to the numbers in Figure 4b). Initially, P2 was located in the magnetosphere and observed a strong (40 nT) and steady magnetic field and hot (~2 keV), tenuous (0.3 cm^{-3}) plasma (see the second and the third frames in Figure 5). After 1423:20 UT, P2 entered

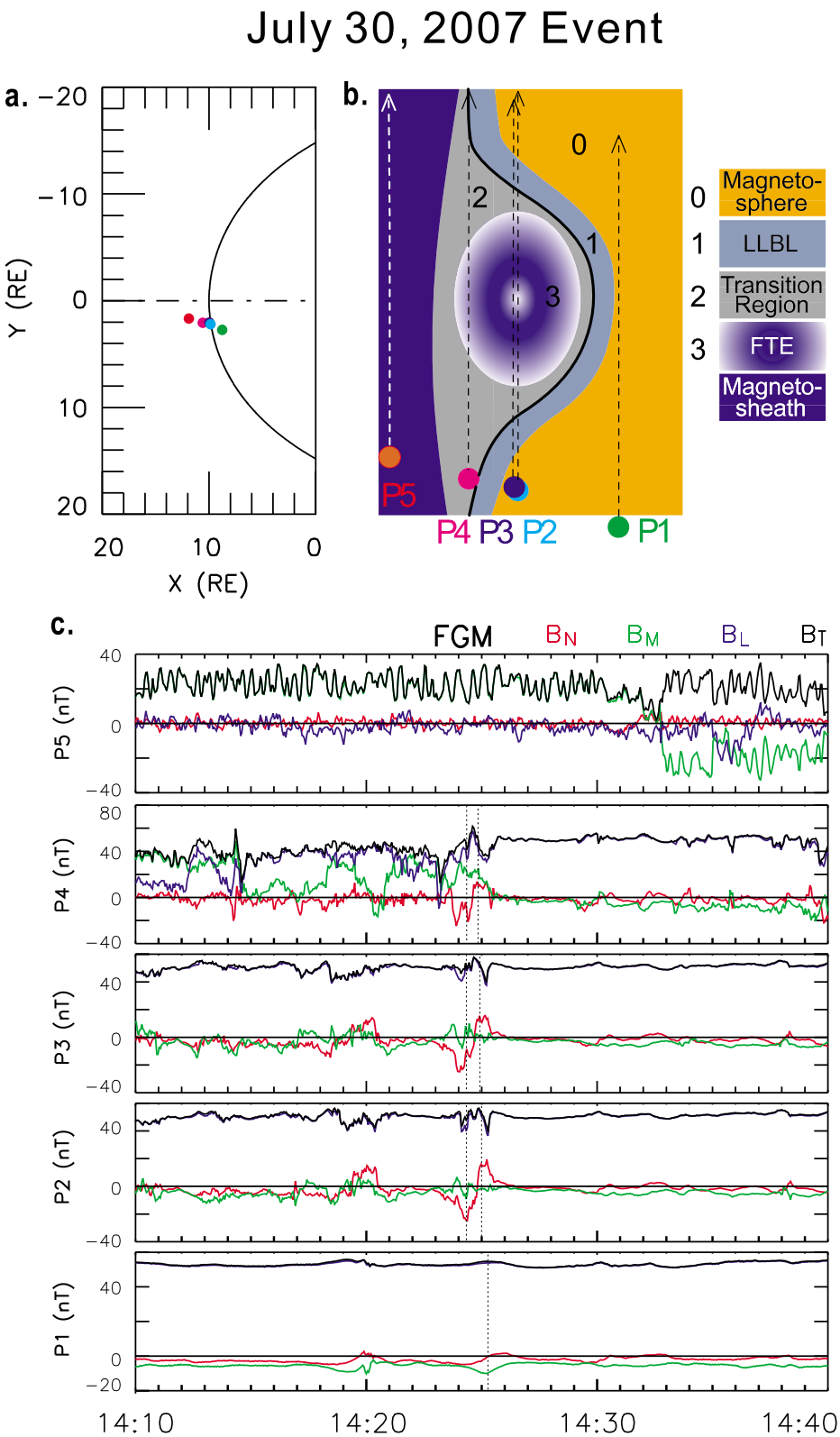

Figure 4. (a) The positions of the five spacecrafts in the GSM X-Y plane for the 30 July 2007 event. (b) A schematic diagram of the trajectories of the five THEMIS spacecrafts projected into the plane transverse to the axis of the FTE. The magnetosphere, the LLBL, a transition region, and the magnetosheath are indicated by color. The black bold curve shows the inner edge of the magnetopause distorted by the passing FTE. (c) An overview of the magnetic field measurements for the 30 July event. All data are presented in a local magnetopause coordinate system (LMN) that is determined from the model of *Shue et al.* [1998] as described in the text.

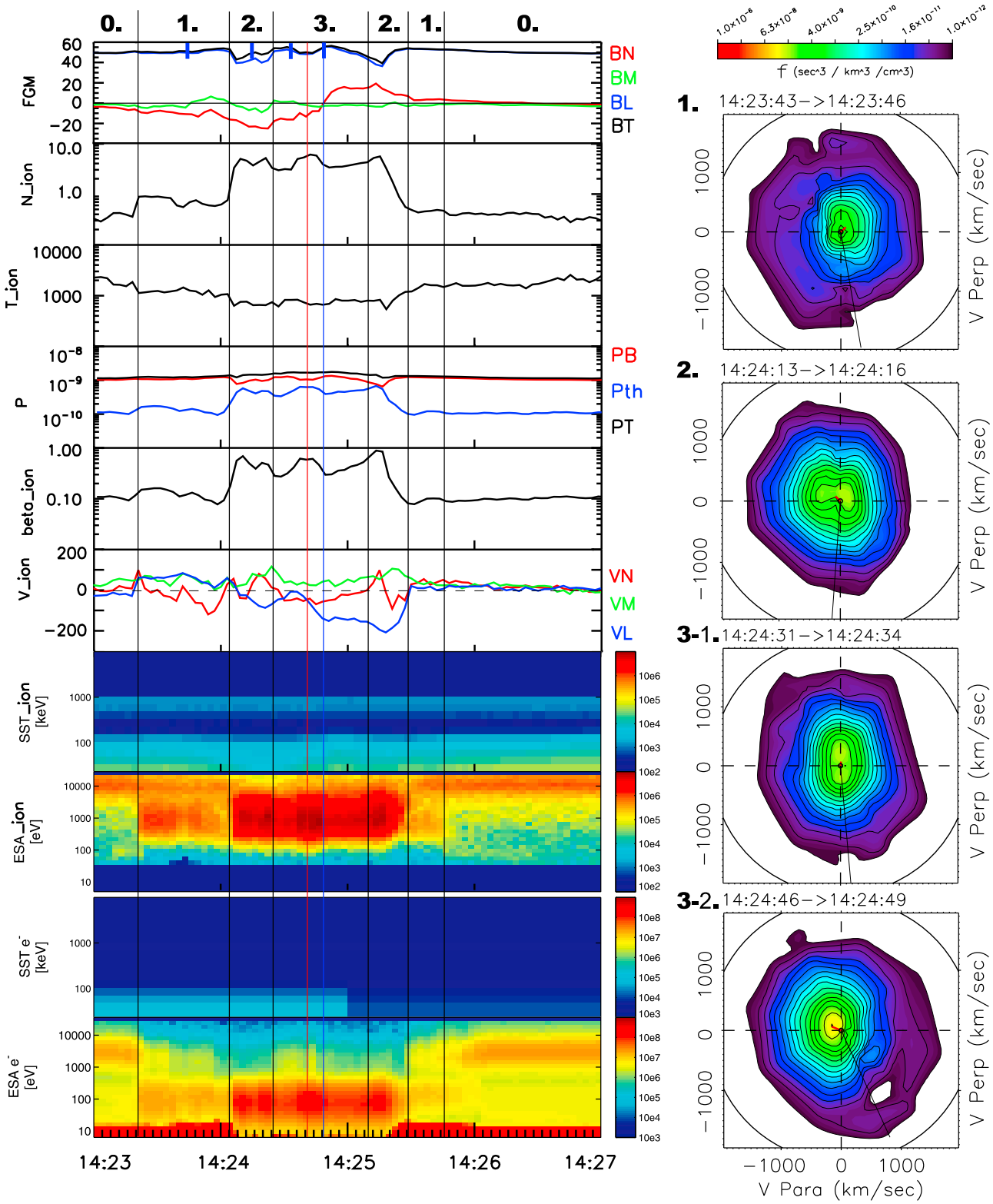
0. 1. 2. 3. 2. 1. 0.
FGM
BN
BM
BL
BT
N_ion
T_ion
P
PB
Pth
PT
beta_ion
V_ion
VN
VM
VL
SST_ion [keV]
ESA_ion [eV]
SST e- [keV]
ESA e- [eV]
14:23
14:24
14:25
14:26
14:27
f (sec^3 / km^3 /cm^3)
1. 14:23:43->14:23:46
2. 14:24:13->14:24:16
3-1. 14:24:31->14:24:34
3-2. 14:24:46->14:24:49
V Perp (km/sec)
V Para (km/sec)

Figure 5

the LLBL region, where hot ((~2 keV) and cold (below 0.5 keV) plasma coexisted (see the bottom four panels as well as velocity distribution (1)). The plasma in region 2 (the transition region or the expanded magnetopause current layer) was colder and much denser than that within the FTE and the LLBL, although high-energy and low-energy particles still coexisted here (see the bottom four frames as well as velocity distribution (2)). Occasionally, there were beams of low-energy ions counterstreaming along the field in this region (velocity distribution (2) in Figure 5). Since these counterstreaming ion beams disappeared within the FTE (region 3), their existence may indicate that reconnection took place later on field lines passing through this region than on field lines that formed the internal structure of the FTE. Reconnection occurring following the formation of an FTE and producing the outer layers of the FTE can be seen in the simulation by *Raeder* [2006]. The recently reconnected field lines could have encircled the FTE half, one or several times, but they probably did not wrap around the FTE along its entire length. Although region 2 surrounds the FTE, it was not intrinsic to the FTE at the time of observation because the plasma and field properties in this region were distinct from those inside the FTE (region 3). After passing through the transition region, P2 encountered the FTE and finally returned to the magnetosphere via the transition region and the LLBL on the trailing side of the FTE.

[26] As P2 passed through the FTE, the measured magnetic and plasma signatures suggest that the FTE was evolving with time. Right at the center of an FTE, the field component along its axis should be dominant and the azimuthal components are weak [e.g., *Kivelson and Khurana*, 1995]. So in passing from the outer layers toward the central region of an FTE, the azimuthal components must finally decrease. In this FTE, as discussed above, the axis was not far from the L direction and B_N and B_M were approximately the two azimuthal components. After the sharp change of the magnetic field at 1424:25 UT P2 entered into the FTE, the B_M component remained small and constant (almost zero), whereas B_N decreased in magnitude, implying that P2 was approaching the central region. As P2 came closer to the core, a decrease in field strength and an increase in thermal pressure as in a C-FTE was observed. The ion velocity distribution was symmetric in the parallel direction (see the velocity distribution (3-1)); the bulk velocity was dominantly perpendicular to the field (the parallel velocity was only a few km/s, whereas the perpendicular velocity was ~80 km/s), indicating that there was no net plasma transport along the magnetic field. About 10 s later (red vertical line in Figure 5), as the spacecraft approached the center of the FTE (where B_N went through 0), the field strength began to increase and the number density to decrease. The ion flow in the L direction, approximately along the axis of the FTE, abruptly increased in magnitude (the sixth frame in Figure 5) in the direction antiparallel to the magnetic field (see a distribution example in 3-2 of Figure 5). Although there is a possibility that the whole FTE structure was moving parallel to its axis, we think it more likely that plasma began to flow along the magnetic field within the structure. When P2 reached the center of the FTE ($B_N = 0$ and $B_M \sim 0$, marked by the blue vertical line in Figure 5), the field magnitude reached its maximum. A field magnitude peak associated with a reversal of B_N on the magnetopause is characteristic of a T-FTE. We suggest that the FTE structure, which initially was a C-FTE, had undergone a temporal change and that midway through the crossing, following the interval of flow along its axis, it had evolved into a T-FTE. Thereafter, the field strength continued to decrease as P2 left the central region and moved toward the opposite edge of the FTE (B_N increased and B_M remained constant and small). Throughout this FTE structure both high- and low-energy particles (combination of electrons and ions from magnetospheric and sheath) were detected (the bottom four frames in Figure 5). We interpret this as evidence that the FTE was encountered not long after its formation at a time when the high-energy particles had not yet escaped from the structure.

[27] In sketching the features of the FTE, we have used the KK95 flux rope model. A desirable feature of this model is that FTEs are embedded within a Harris current sheet. We have adopted the model here ignoring the fact that the conditions external to the FTE are not those assumed (the external pressure is imposed by a combination of magnetic and thermal pressure, and the field orientation is not that of a Harris neutral sheet). Furthermore, although the model assumes equilibrium, which appears not to be the situation for our C-FTE event. It is then understandable that the model fails to represent the details of this FTE.

[28] Despite its inadequacy, we adopt the KK95 model for the inner portion of the FTE because it does reflect to some extent the way in which the structure is distorted by external forces. We select the P2 data from 1424:25 to 1425:05 UT and the P3 data from 1424:20 to 1425:00 UT to fit to the KK95 model. The KK95 model has no pressure gradient along the magnetic field so the two azimuthal components, B_1 and B_2, are independent of gradients in the thermal pressure. Only the B_3 component, but not B_1 and B_2, are modified by thermal pressure gradients. Consequently, we first fit the

Figure 5. The plasma and magnetic field data from P2 for the 30 July 2007 event. From top to bottom the plots on the left show the magnetic field in an LMN coordinate system (B_N in red, B_M in green, B_L in blue, and the field magnitude B_T in black), the ion number density, the ion temperature, the magnetic pressure (in blue), thermal pressure (in red) and the total pressure (in black), and the ion beta and the ion bulk velocity also in LMN coordinate system (V_N in red, V_M in green, and V_L in blue). The bottom four frames display the ion and electron energy spectra from SST and electrostatic analyzers, respectively. On the top of the plots, "0" stands for the magnetosphere, "1" stands for LLBL, "2" stands for the transition region between the FTE and LLBL, and "3" stands for the FTE. The red vertical line marks the beginning of the flow along the FTE axis, and the blue vertical line denotes the reversal point of the B_N component. Four distinct velocity distributions from different regions are shown on the right, and their times correspond to the short blue lines on the top of the plots on the left. The red lines in the center of the distribution plots indicate the ion bulk velocities, and the velocity distribution planes are determined by this bulk velocity and the magnetic field (X axis).

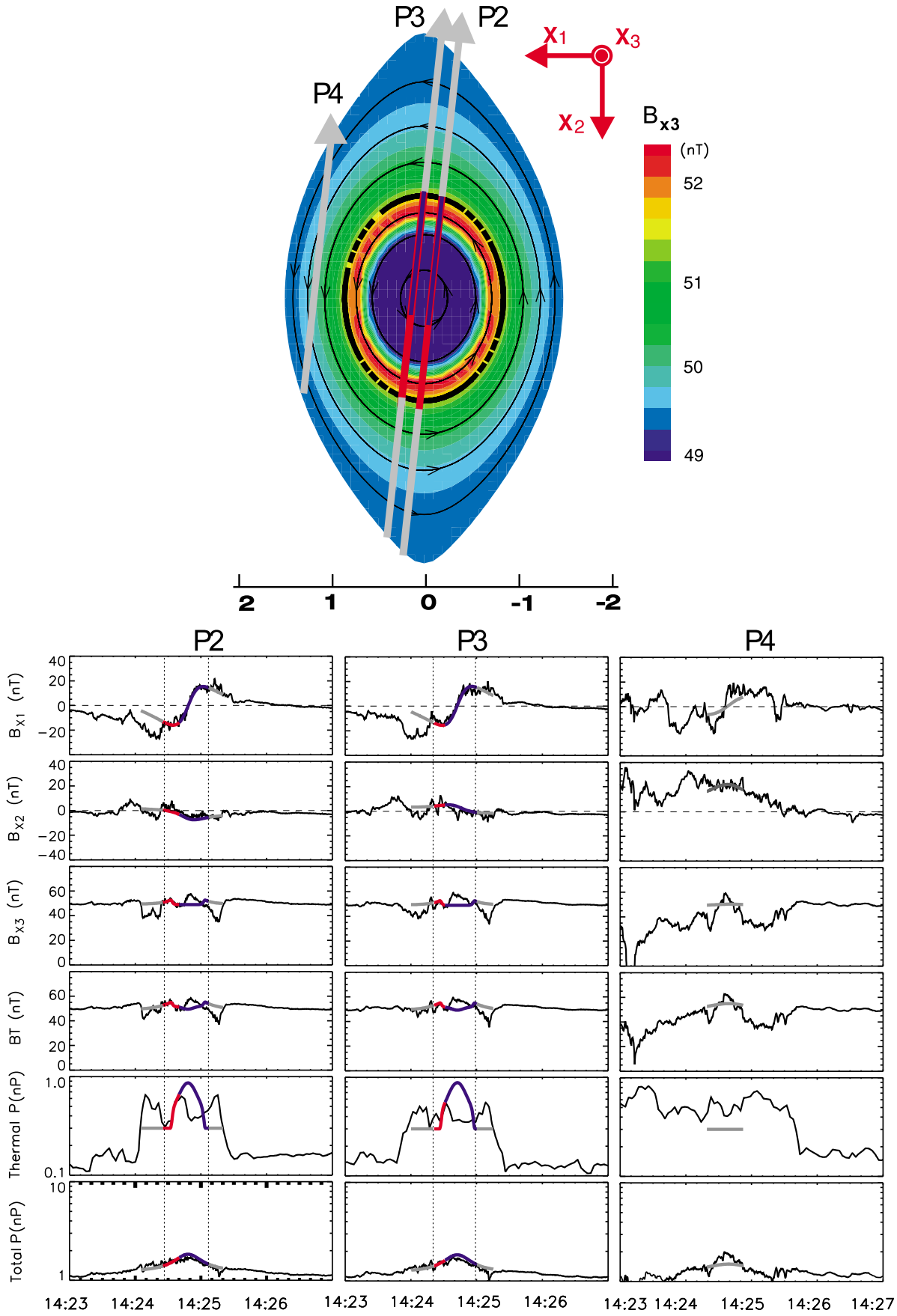
P3
P2
P4
X1
X3
X2
Bx3
(nT)
52
51
50
49
2
1
0
-1
-2
P2
P3
P4
BX1 (nT)
BX2 (nT)
BX3 (nT)
BT (nT)
Thermal P(nP)
Total P(nP)
14:23
14:24
14:25
14:26
14:27

Figure 6

perturbations in B_1 and B_2 during the time interval selected and then attempt to reproduce the perturbations of B_3 by modifying the thermal pressure profile, but we fail to find a good fit. We assume that the satellites crossed the FTE along straight lines because the velocity remained almost constant in the N and M directions. The detailed fitting technique is discussed by *Zhang et al.* [2008]. The upper plot in Figure 6 shows the B_3 profile produced by the KK95 model with $B_{2,\infty}$ = 16 nT, $B_{3,\infty}$ = 49 nT, L = 1200 km, ε = 1.0, γ = 200, and κ = −16. The best fit for the two azimuthal components, B_1 and B_2, is used to establish the orientation of the axis of the flux rope as (0.0, 0.02, 0.99) in the LMN coordinate system. Thus, the axis was close to the L axis of the system. The projections of the spacecraft trajectories of P2, P3, and P4 start from bottom to top and they are basically against $\mathbf{x}_2$. The observed and modeled magnetic field and pressure at the three spacecrafts are plotted in the bottom three plots. From top to bottom of each plot are displayed B_1, B_2, B_3, B_T, the thermal pressure, and the total pressure. The observed data are plotted as thin curves, and the modeled data are plotted as thick lines. Our model well reproduced the slowly varying portion of the observed B_1 and B_2 signatures between two vertical lines at P2 and P3, during which time the spacecraft trajectories lie within the oval shown as a dashed curve in the upper plot, that is, in the inner region of the modeled flux rope. The traces are colored to indicate whether or not the model gives a reasonable fit along portions of the trajectory. The red portions of the trajectory indicate that all the modeled data, including all the components of the field and the pressure, match the observations reasonably well; blue portions of the trajectory are those for which B_1 and B_2 are modeled reasonably well but the observed B_3 and B_T suddenly increase and exceed the modeled values. The observed thermal pressure suddenly decreases and becomes significantly smaller than the modeled values, thus, maintaining pressure balance in the presence of the enhanced magnetic pressure. The observed total pressure in this region is not far from its value in our model. Since the KK95 model is a static model in which the field and plasma pressures are balanced and the flux rope structure does not change with time, it is plausible to propose that during intervals corresponding to the red curves the FTE was not changing in time and was close to equilibrium. The deviation of the field magnitude and pressure from the model as the spacecraft moved along the blue curves, times during which the plasma data show that strong field-aligned plasma flows developed, is consistent with the suggestion that the FTE structure was evolving. The gray traces show the data in the outer layers of the flux rope that we have referred to as a "transition region." This region possibly corresponds to the newly formed outer layers of the FTE or the layers affected significantly by the ambient fields and plasma, and we cannot model the field and plasma in this region.

4.2. A T-FTE on 20 May 2007

[29] A representative T-FTE event, observed by THEMIS on 20 May 2007, was found to be in steady state and has been extensively discussed by *Sibeck et al.* [2008], *Lui et al.* [2008a, 2008b], and *Zhang et al.* [2008]. For comparison with the detailed description of the C-FTE above, here we explore the characteristic field and plasma properties within this T-FTE structure. The event was encountered on the dusk flank of the magnetopause at about 2 R_E above the equator (Figure 1a as well as Figure 7a), and magnetic disturbances were recorded by instruments on board all the five THEMIS spacecrafts. Figure 7c displays an overview of the magnetic field data with the plots ordered from top to bottom by the radial distance of the spacecraft starting from the most distant, i.e., from P5 to P4, P3, P2, and finally to P1 (Figure 7b). Bipolar signatures are seen around 2202 UT in the B_N components. *Zhang et al.* [2008] inferred the trajectories of all five spacecrafts relative to the FTE, which are schematically shown in Figure 7b. P3 crossed through the center of the flux rope and recorded the strongest core field. The single, strong peak of field magnitude associated with the bipolar B_N identifies this event as a "typical FTE" (T-FTE) on the basis of the working definition in this paper. P5 and P4 remotely sensed the magnetic perturbations in the magnetosheath when the FTE was moving along the magnetopause; they also recorded the magnetosheath conditions with B_L = −8 nT and B_M = 15 nT before and after encountering the FTE. P2 was initially located in the magnetosphere and then grazed the magnetospheric-side edge of the FTE. P1, the innermost spacecraft, moved from and finally back to the magnetosphere via the transition region between the FTE and magnetosphere [*Zhang et al.*, 2008] and recorded a dip of field magnitude near the center of the bipolar normal field perturbation much like the signature of a crater FTE but arising from the different field and plasma structure [*Sibeck et al.*, 2008]. The local magnetospheric field recorded by P1 pointed northward and dawnward with B_L = 20 nT and B_M = −20 nT. The magnetic shear angle between the sheath field and the local geomagnetic field was about 163° (the associated IMF clock angle was 118°). The core field significantly exceeded the field magnitude in the background magnetosphere as required for its associated pressure to balance the sum of the external pressure and the inward force of the curved flux tubes that surround the core.

[30] Figure 8 gives the plasma data from P3 that went through the FTE's center. Initially, P3 was located in the magnetosphere (region marked 0 in Figure 8) where a hot and tenuous plasma was observed. Then it briefly moved into the LLBL region and detected plasma with both hot and cold components (see the bottom four frames in region 1 and velocity distribution (1) in Figure 8). After crossing the inner edge of the magnetopause at about 2159:10 UT, P3

Figure 6. Fits to the 30 July 2007 C-FTE event. The upper plot is the modeled core field component contour. The trajectory projections of P2, P3, and P4 were inferred from a fit of the B_1 and B_2 components within the dash oval line. Red marks portions of the trajectories over which the model well reproduced all the three components of the observed fields; on portions of the trajectories marked in blue, the two azimuthal components B_1 and B_2 are modeled reasonably well, but the core field component is poorly modeled. Intervals colored gray crossed the outer layers of the flux rope (transition region) where the model is not appropriately designed to represent the field. The bottom three plots show the observed and modeled fields, thermal pressure, and total pressure at P2, P3, and P4, respectively.

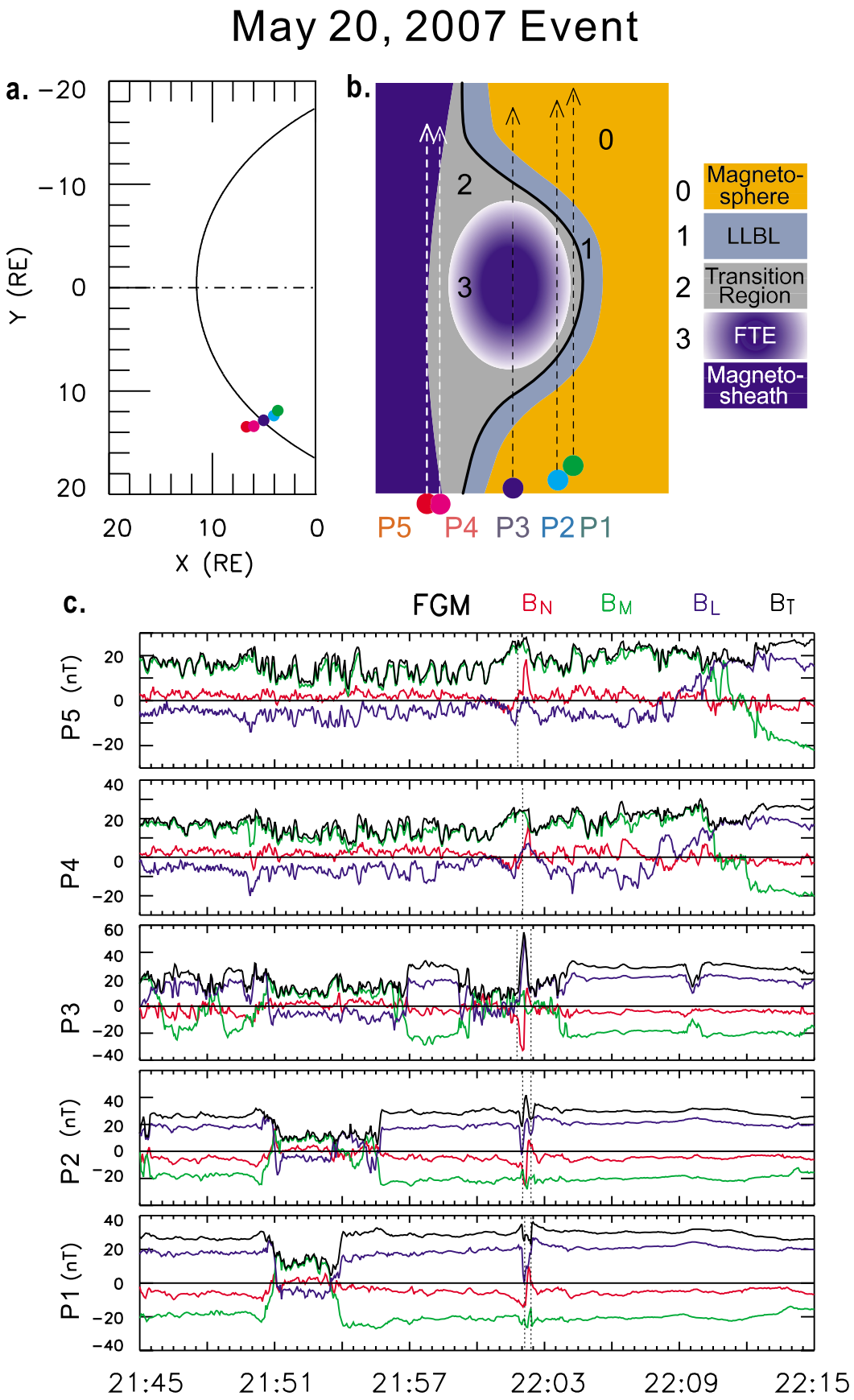

Figure 7. As in Figure 4 for the event on 20 May 2007. (a) The positions of the five spacecrafts. (b) A schematic diagram of trajectories of the five THEMIS relative to the FTE. (c) Plots of the magnetic field.

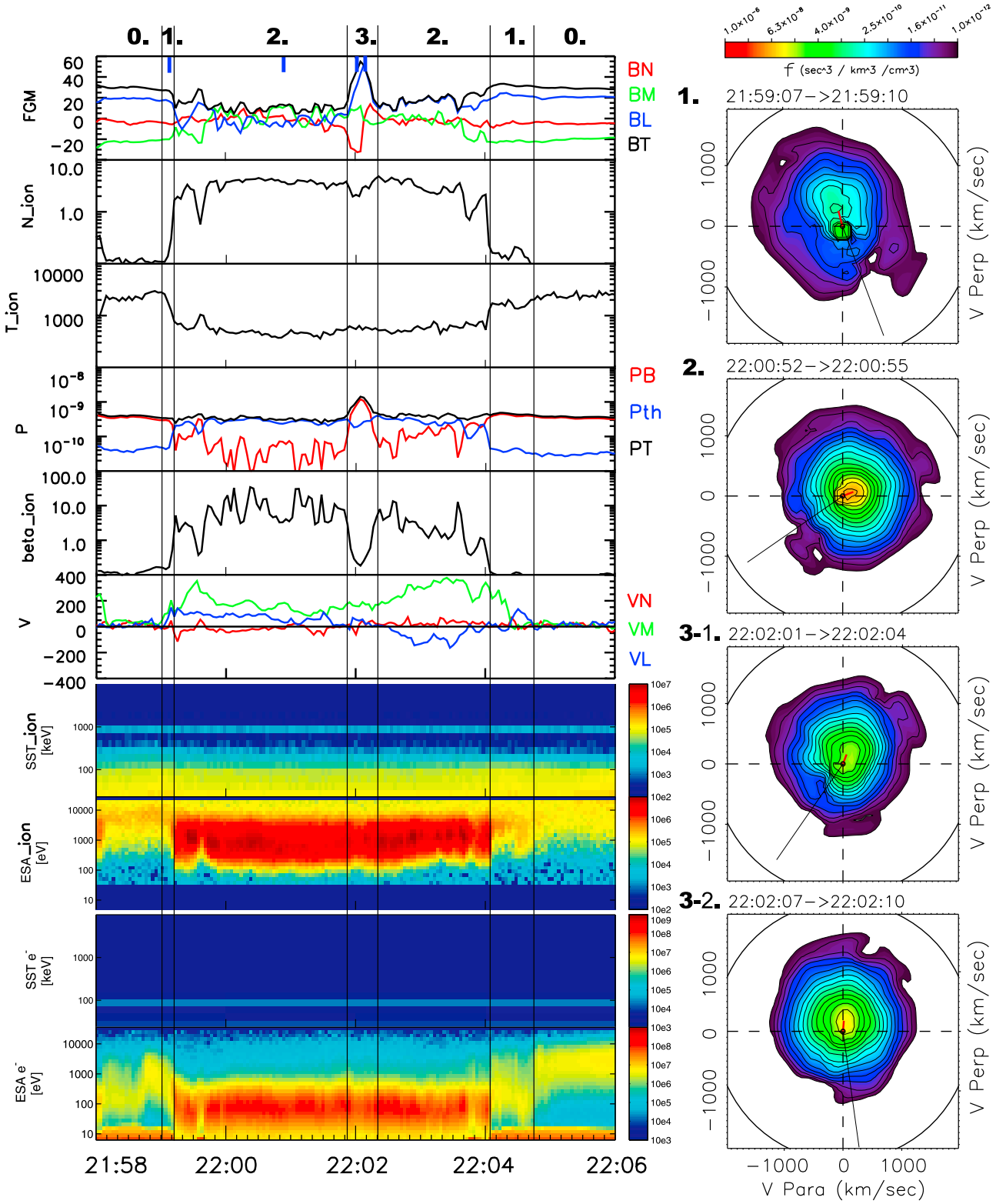

Figure 8. As in Figure 5, the plasma and field data from P3 for the 20 May 2007 event.

passed through an indentation in the magnetopause, which was filled mainly with low energy and dense sheath particles (velocity distribution (2)) and which we refer to as the "transition region." The FTE was embedded within this indented region (or expanded magnetopause current layer). Finally, P3 returned to the magnetosphere via the LLBL. The trajectory of P3 in Figure 7b indicates its encounters with the above mentioned distinct regions.

[31] Although our interpretation of the data from P1 and P2 implies that the inner edge of the magnetopause has been locally distorted into the magnetosphere, we can confirm the distorted configuration by applying the MVA technique to the 0.25 s resolution magnetopause crossing data of P3 to estimate the normal direction of the magnetopause. Just before and soon after the encounter of the FTE, from 2159:10 to 2159:17 UT and from 2203:35 to 2203:40 UT, respectively, P3 crossed the magnetopause twice. The MVA technique applied to these periods gave two minimum variance directions: (0.773, 0.597, 0.214) and (0.653, 0.728, 0.209) in the GSM coordinate system. The estimates are robust because the eigenvalues $\lambda 1$, $\lambda 2$, and $\lambda 3$ in the MVA, corresponding to the maximum, intermediate, and minimum variance directions, respectively, for the two magnetopause crossings, are well separated in magnitude having values of 56.0, 17.9, 0.8 and 26.2, 7.9, 0.3 for the two cases. The undisturbed local magnetopause normal was estimated to be along (0.692, 0.715, 0.092) in GSM by the *Shue et al.* [1998] model. That the undisturbed normal direction lies between the two normal directions determined by the MVA technique ahead and behind the FTE supports the suggestion that the local magnetopause was indented as shown in Figure 7b as well as in Figure 12 in the study of *Zhang et al.* [2008].

[32] *Zhang et al.* [2008] estimated the thermal pressure gradient (6×10^{-17} N/m^3) within this FTE and found that it was negligible compared with the magnetic pressure gradient (4×10^{-16} N/m^3). They succeeded in fitting the multi-spacecraft magnetic field observations through this event to a force-free solution of the KK95 model (set $P_o = 0$ in equations (2) and (3)). On the basis of the fit result, they inferred the spacecraft trajectories relative to the flux rope and concluded that P3 crossed the center of the FTE and that the FTE was really a T-FTE. This FTE did not make direct contact with the magnetosphere (or the low latitude boundary layer); it was embedded in a "transition region" that forms the ambient background for the FTE [*Sibeck et al.*, 2008; *Zhang et al.*, 2008]. The cross-sectional map and axis direction of this event were also reproduced successfully by *Lui et al.* [2008a, 2008b] using the Grad-Shafranov reconstruction technique. *Lui et al.* [2008a] found that the core field direction was along (−0.4241, 0.1134, 0.8985) in Geocentric Solar Ecliptic (GSE) coordinates. We have rotated this solution into GSM coordinates to obtain (−0.4241, −0.247, 0.871), which, differs from the orientation along (−0.350, −0.264, 0.899) in GSM found by *Zhang et al.* [2008] by less than 5° (*Lui et al.* [2008b] state that the orientation of the axis of the FTE was along (−0.4241, 0.1134, 0.8985) in GSM coordinates, which we believe to be a typo). The basic but critical assumption and precondition for the applicability of the Grad-Shafranov technique is that FTE should be in steady state, and so the excellent match between the observed and reproduced data in this event (by both *Lui et al.* [2008a] and *Zhang et al.* [2008]) is consistent with our assertion that the FTE was in a steady state.

[33] Various features of the plasma in this T-FTE were obviously different from those within the C-FTE that we studied. The ion flow within this FTE was perpendicular to the axis of the FTE; velocity distributions (3-1) and (3-2) show that there were no strong ion bulk flows along field lines, implying that plasma transport along its axis was weak. For comparison's sake, we emphasize that the significant plasma transport developed midway through the passage of the C-FTE discussed in the previous section. This T-FTE contained no high-energy plasma, and the sheath-origin low-energy plasma was a bit more tenuous than in the magnetosheath (see the eight and ninth frames in Figure 8). Since reconnection should have led to the coexistence of high- and low-energy particles within the FTE, the absence of high-energy particles within the structure suggests that THEMIS encountered it well after its formation and that the higher-energy particles of the distribution had had time to escape leaving the FTE in a steady or slowly evolving state.

5. Statistical Studies

[34] In this section we consider how the two classes of FTE we have identified relate statistically to the IMF and solar wind conditions. We also characterize aspects of their internal properties in order to gain insight into their formation and to test our model of evolution of C-FTEs to T-FTEs. As we mentioned previously, the signature of a C-FTE cannot be mimicked by any linear path through a T-FTE, whereas a spacecraft may register a T-FTE signature if its path grazes the outer layers of the C-FTE. In order to compare the properties of 23 C-FTEs in our data set with T-FTE events, we must be confident that we have properly identified unambiguous T-FTEs as we select them from among the 599 events of this study. We next describe the approach used for that purpose.

5.1. Event Reselection

[35] Minimum variance analysis (MVA) of the magnetic field is widely used to infer the characteristic directions of magnetic structures or transition layers in plasmas [*Sonnerup and Cahill*, 1967]. This technique identifies three orthogonal eigen directions: **i**, **j**, and **k** corresponding to the directions of maximum, intermediate, and minimum magnetic fluctuations, respectively. When applied to FTEs, the technique is generally used to determine the directions of the principal axes [e.g., *Elphic et al.*, 1980; *Xiao et al.*, 2004]. Our desire is to use MVA to estimate the impact parameter of a spacecraft relative to an FTE.

[36] We start by recognizing that in a cylindrical coordinate system aligned with the core field, $B_{\rm axis}$ a flux rope contains azimuthal (B_φ) and radial ($B_{\rm r}$) field components. If the cross section of an FTE is not extremely oblate, the radial component $B_{\rm r}$ should be significantly weaker than the other two components. For paths through the center of the FTE, $B_{\rm axis}$ experiences a peak, B_φ reverses its direction across the FTE, and $B_{\rm r}$ changes little. Thus, the minimum variance direction **k** should be close to the radial direction and the averaged field components along **k**, $\langle B_k \rangle$, should be small. If the path does not go through the central region, $B_{\rm r}$, instead of B_φ, reverses its direction, and the minimum variance direction **k** may even be in the azimuthal direction. Since B_φ can be very large, $\langle B_k \rangle$, the averaged field components along **k** will not be small for impact parameters of order the scale of the FTE. Thus, $\langle B_k \rangle$ is a useful parameter for estimating whether or not the impact parameter is small. Normalization is critical. In order to make the index comparable for different events, we have normalized $\langle B_k \rangle$ by the

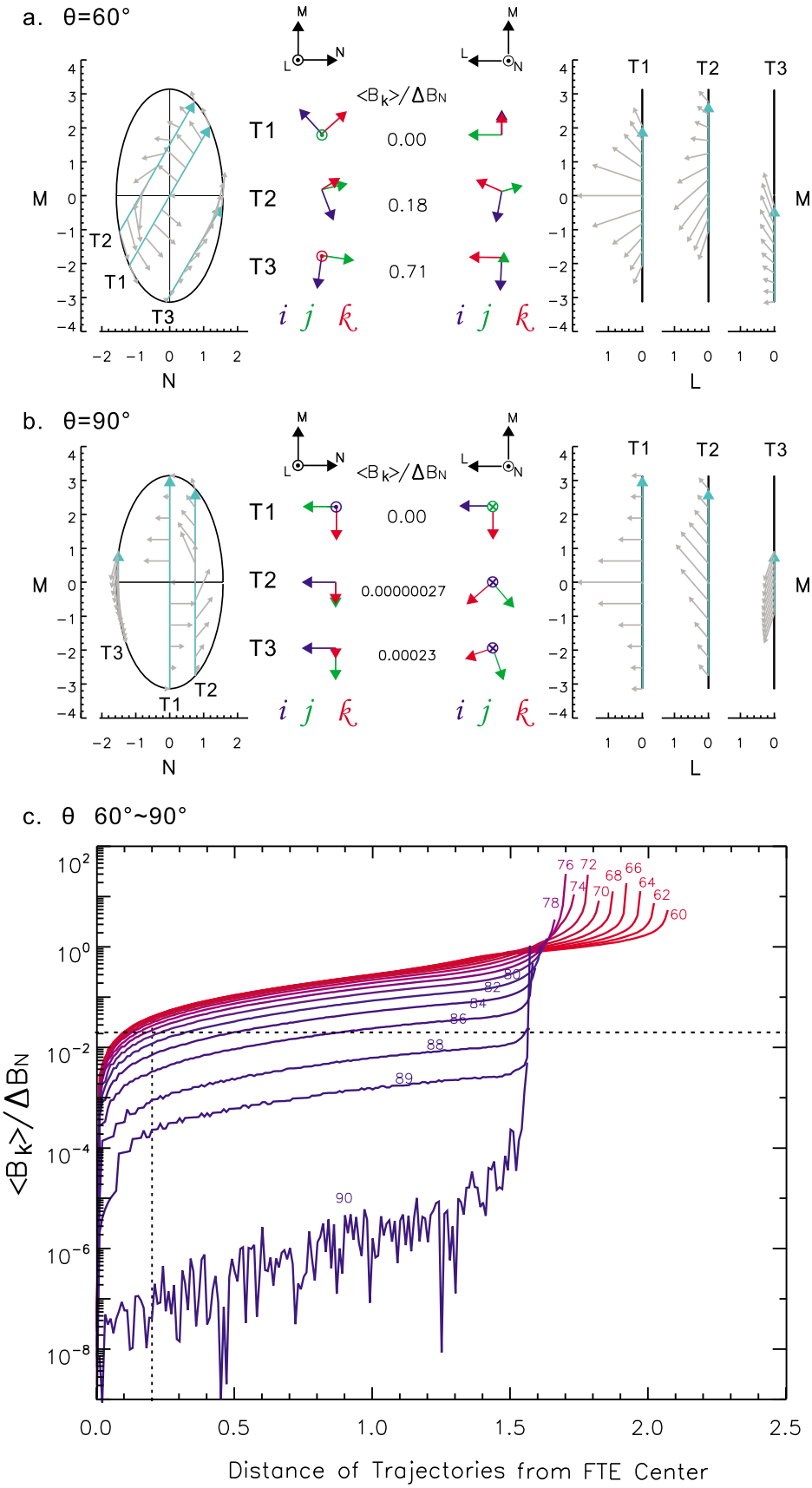
a. θ=60°
b. θ=90°
c. θ 60°~90°
<B_k>/ΔB_N
0.00
0.18
0.71
0.00
0.00000027
0.00023
T1
T2
T3
M
N
L
i j k
Distance of Trajectories from FTE Center

Figure 9

magnitude of bipolar perturbations on the magnetopause: $\langle B_k \rangle / \Delta B_N$, and we propose this quantity as a candidate index that is linked to the impact parameter of the spacecraft trajectory. For example, we applied this technique to the observations in the 20 May 2007 event. On the basis of the data of P3, which crossed the center of the FTE, the core field direction obtained from the MVA was (−0.260, −0.149, 0.954) in GSM [*Zhang et al.*, 2008], which deviated by only 8.9° from our model result. The indices, $\langle B_k \rangle / \Delta B_N$, for the data of three satellites, P3, P2, and P1, which crossed the FTE structure with increasing impact parameters, increase significantly from 0.07 to 0.35 and 0.99, indicating that the index closely relates to the impact parameter.

[37] In order to test the usefulness of the suggested index, we use the KK95 model parameterized to fit the 20 May T-FTE event. We set $B_{2,\infty}$ = 24 nT, $B_{3,\infty}$ = 0 nT, ε = 1.0, and P_o = 0 nPa. We take paths through this model using different values of the angle θ and the impact parameter d and apply minimum variance analysis to the field values inferred. Here θ refers to the angle between the trajectory projection and the short axis of the flux rope, and d stands for the distance from the center of the flux rope to the projection of the trajectory on the cross-section plane, as shown in Figure 3. Figure 9a shows the variation with d of the index $\langle B_k \rangle / \Delta B_N$ for $\theta = 60°$. The left- and the right-hand columns of Figure 9a show the magnetic field along three different trajectories projected onto the M-N plane and the L-M plane, respectively. As the impact parameter d increases (T1: $d = 0$; T2: $d = 0.75$; T3: $d = 1.5$), the index $\langle B_k \rangle / \Delta B_N$ increases significantly (T1: 0; T2: 0.18; T3: 0.71), implying that the index is a monotonic function of the impact parameter. However, quantitative values of the proposed index depend on θ. As shown in Figure 9b, if $\theta = 90°$, for values of d from 0 to 1.5, the index $\langle B_k \rangle / \Delta B_N$ remains very small and is not sensitive to the impact parameters. In these two tests, we also noticed that there is not a principal MVA axis along the axis of the flux rope unless the spacecraft path goes exactly through the center of flux rope, indicating that MVA does not provide a good estimate of the core field direction of an FTE.

[38] In Figure 9c, we show values of $\langle B_k \rangle / \Delta B_N$ as a function of impact parameter for values of θ between 60° and 90°. The abscissa of Figure 9c shows the impact parameter d, and the ordinate is the index $\langle B_k \rangle / \Delta B_N$. Colors vary from red to blue corresponding to values of θ from 60° to 90°. For each trace, as d approaches zero, the index $\langle B_k \rangle / \Delta B_N$ decreases sharply. For a large range of impact angles, a strict requirement $\langle B_k \rangle / \Delta B_N < 0.02$ would imply that the impact parameter is less than 0.2. The half width of the structure is 1.57 in width and 3.14 in length, so impact parameters less than 0.2 come within 13% of the center. It is evident from Figure 9c that small values of the index do not necessarily imply small impact parameters when the spacecraft path corresponds to θ near 90°. Fortunately, two velocities determine the θ of a trajectory: one is the velocity of flux rope along the magnetopause, which can vary from several tens of kilometers per second to several hundreds of kilometers per second (the C-FTE on 30 July 2007: 65 km/s; the T-FTE on 20 May 2007: 170 km/s); the other is the velocity of magnetopause, which can typically be several tens of kilometers per second (e.g., 40 km/s determined by *Haaland et al.* [2004]) and can change dramatically. Thus, in real events, θ is likely to deviate significantly from 90°, in which case the criterion $\langle B_k \rangle / \Delta B_N < 0.02$ most likely means that the pass came relatively close to the center of the flux rope. We, therefore, use this criterion to select a subset of T-FTEs for which there is a high probability that THEMIS passed near the center.

[39] We selected 35 of the 599 T-FTE-like events on the basis of the strict criterion $\langle B_k \rangle / \Delta B_N < 0.02$. The positions at which they were encountered are plotted in blue dots in Figure 1b. Despite satisfying the selection criterion, these events may not all be T-FTEs. Indeed, it is even possible that all the 35 events were C-FTEs and that spacecraft grazed their outer layers and registered T-FTE signatures. Additional analysis of the selected events is called for.

[40] In designing a further test, we note that the maximum field magnitude on trajectories through a C-FTE should be somewhat larger for trajectories that register a C-FTE signature than on grazing trajectories that yield T-FTE-like signatures. As a test of this hypothesis, we used the model that fit the initial portion of the C-FTE of 30 July 2007 discussed in this paper. The parameters of the fit are $B_{2,\infty}$ = 16 nT, $B_{3,\infty}$ = 49 nT, L = 1200 km, ε = 1.0, γ = 200, and κ = −16. For a range of θ between 60° and 90°, we obtained the maximum field along trajectories as a function of impact parameter. The distribution of maximum fields for the two classes of signatures is plotted in Figure 10a. The averages of the maximum field magnitudes (normalized by the asymptotic field strength at large $\mathbf{x}_1$) for C-FTE signatures and T-FTE-like signatures are 1.09 (standard deviation: 0.0002) and 1.05 (standard deviation: 0.0007), respectively. The field strengths for T-FTE-like events are statistically smaller than C-FTE-like events as shown in Figure 10a.

[41] Let us apply the model results to the 35 events identified as T-FTEs. If a significant fraction of the nominal T-FTE signatures represent measurements on grazing paths across C-FTEs, the maximum field strength in these 35 events should be on average smaller than for the 23 events with clear

Figure 9. Tests of the relation between the impact parameter of a spacecraft trajectory and the ratio $\langle B_k \rangle / \Delta B_N$, where $\langle B_k \rangle$ is the average value of the field component along the minimum variance direction **k** and ΔB_N is the largest magnetic field perturbation in the magnetopause normal direction. (a) Here $\theta = 60°$. The distances of the three trajectories, T1, T2, and T3, from the center of the flux rope are 0, 0.75, and 1.5, respectively, in unit of the scale length. The ratios $\langle B_k \rangle / \Delta B_N$ along these trajectories are 0.00, 0.18, and 0.71, respectively. The left frame shows trajectories and their associated magnetic fields in the M-N plane, the right frame shows them in the L-M plane, and the colored vectors in the middle display the projections of the three orthogonal eigenvectors (**i**, **j**, **k**) in the M-N plane and the L-M plane, respectively. The axis of the flux rope is along the L direction, and the normal to the magnetopause is along the N direction. (b) As in Figure 9a but for $\theta = 90°$. The distances of the three trajectories are still 0.00, 0.75, and 1.50, while the ratios, $\langle B_k \rangle / \Delta B_N$, change but remain small. (c) The ratio $\langle B_k \rangle / \Delta B_N$ as a function of the distance of trajectory to the center of the flux rope. The colors of curves varying from red to blue are associated with θ changing from 60° to 90°.

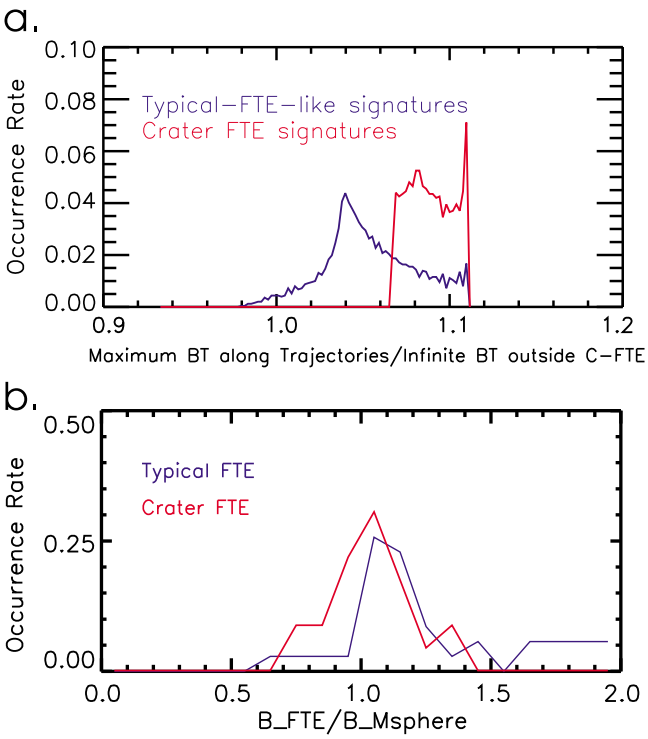

Figure 10. (a) The distribution of the maximum magnetic field strengths along trajectories which cross a model C-FTE for θ between 90° and 60° and varying impact parameters. We normalize the field strengths by the asymptotic field strengths at large $\mathbf{x}_1$. When a trajectory goes through a C-FTE, it can register either C-FTE signatures or T-FTE-like signatures. The red (blue) curve in this plot is for trajectories that yield C-FTE (T-FTE) signatures. (b) The distribution of the maximum magnetic field strengths observed inside 23 real C-FTEs (red) and the 35 T-FTE-like events (blue), which are normalized by the background magnetospheric field strengths.

C-FTE signatures. The occurrence possibilities as a function of the observed maximum field magnitudes (normalized by the background geomagnetic field) inside 23 C-FTEs and inside the 35 candidate T-FTEs are shown in Figure 10b. The averages of the normalized maximum field magnitudes for C-FTEs and T-FTEs are 0.97 (standard deviation: 0.027) and 1.26 (standard deviation: 0.112), respectively. The field strengths differ relatively little but are slightly larger for T-FTE-like events than for C-FTEs, which supports the expectation that most of the 35 events selected as T-FTEs are unlikely to be C-FTEs encountered on grazing orbits.

[42] A larger set of nominal T-FTEs can be obtained by weakening the event selection criterion. The criterion $\langle B_k \rangle / \Delta B_N < 0.1$ (instead of <0.02) yields more than 140 events as nominal T-FTEs. We find that for this much larger set of events the maximum fields are also systematically stronger than the maximum fields inside the 23 C-FTEs, an indication that most of the events we have identified in Figure 1 are true T-FTEs and that they are much more common than C-FTEs.

5.2. Comparison Between C-FTEs and T-FTEs

[43] Since FTEs are thought to be generated on the dayside magnetopause by magnetic reconnection that is controlled by the IMF conditions, it has been suggested that the different forms of FTE (C-FTE and T-FTE) are related to different IMF conditions. In this section, we analyze the IMF distribution for the two types of FTEs. The solar wind is monitored by an Advanced Composition Explorer (ACE), Geotail, or Wind, located in the solar wind well away from the magnetopause. For our study, the solar wind plasma and IMF data have been mapped to the front of the magnetopause by the technique established by *Weimer et al.* [2002, 2003] and *Weimer* [2004], and we use these data to examine the relation of FTE structure and the properties of the solar wind. Figure 11a gives the associated IMF clock angles for the C-FTEs (in red) and the T-FTEs (in blue). It is evident that, for both types of FTEs, the IMF clock angles scatter within the range of ~50° and 180°. The angular distributions differ little between the T-FTEs and the C-FTEs, although there are more cases of close to southward orientation for the set of T-FTEs. The IMF clock angle distributions by the magnetosheath ion beta are shown in Figure 11b. The ion beta randomly varies between 0 and 2 and there is also no clear association of ranges of beta and the two types of FTEs. The comparison shows that neither the IMF clock angle nor the solar wind beta relate systematically to differences of structure (C-FTE or T-FTE).

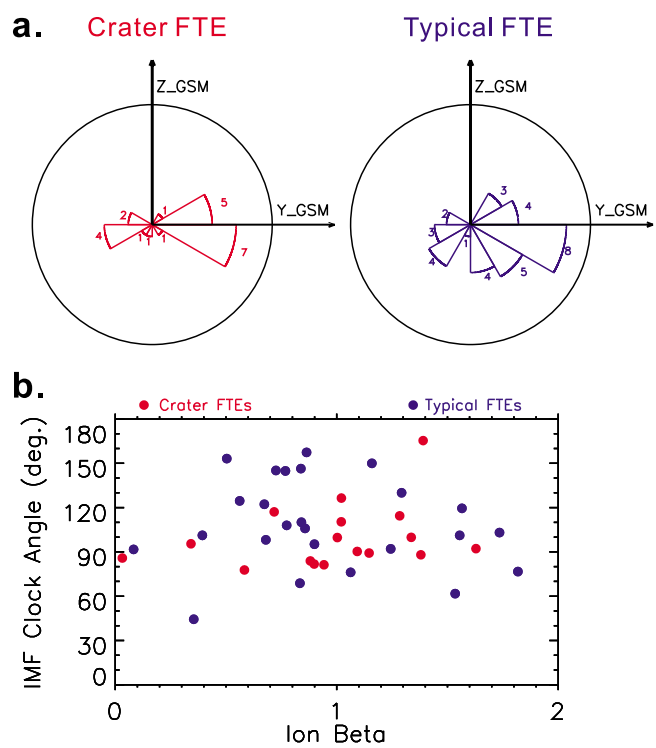

Figure 11. (a) The IMF clock angle distributions for the 22 C-FTEs (red) and the 34 T-FTEs. (b) The IMF clock angles for the C-FTEs (in red) and for T-FTEs (in blue) are plotted as a function of the magnetosheath ion beta. All the IMF and the solar wind data were observed by ACE, Geotail, or Wind when they were located in the solar wind. All the data have been shifted to the front of the magnetopause.

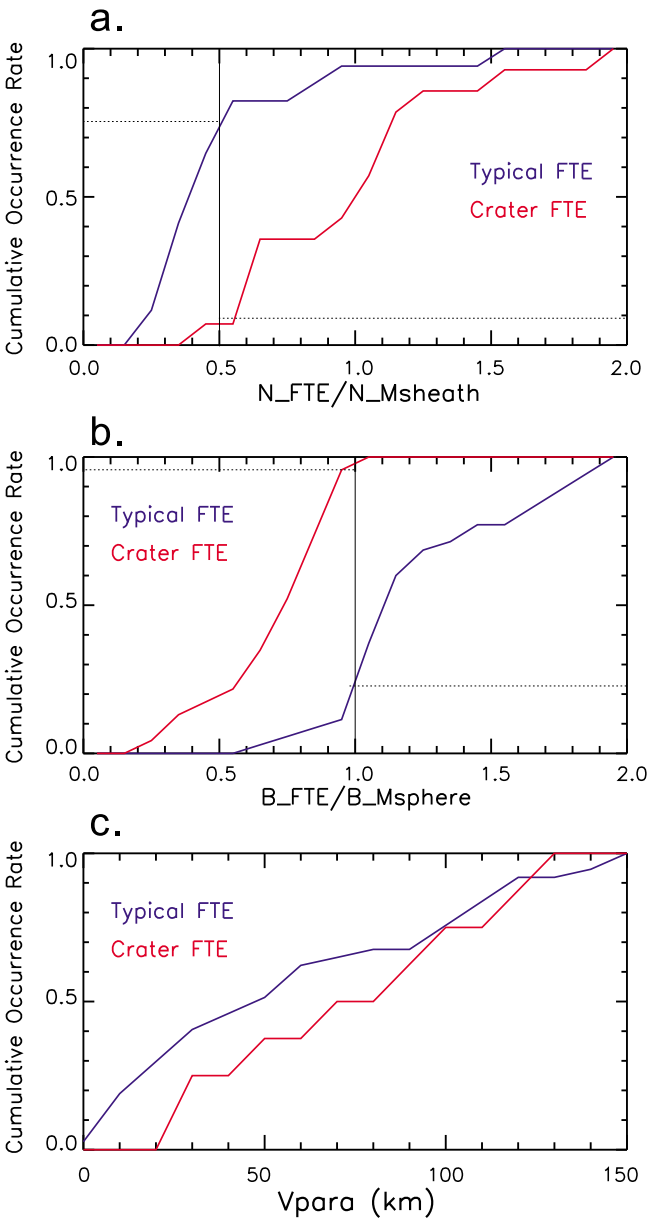

Figure 12. The cumulative distributions of FTEs (typical FTEs in blue and C-FTEs in red) by (a) the ratio of number density inside FTE to that in the background magnetosheath, (b) the ratio of field strength inside FTE to that in the background magnetosphere, and (c) the parallel ion bulk velocity inside FTEs. The internal parameters of an FTE are sampled within 12 s of the reversal point of B_N. The background sheath or magnetospheric properties are the averaged values within 60 min around FTE (30 min before and 30 min after).

[44] The plasma and field properties in the core regions of the 35 T-FTEs and 23 C-FTEs are compared in Figure 12. Figure 12a shows the cumulative distributions of FTEs as functions of the ratio of the number density inside the FTEs to that in the magnetosheath ($N_{FTE}/N_{MSheath}$). The red curve is for C-FTEs, and the blue is for T-FTEs. The background magnetosheath number density $N_{MSheath}$ is either measured on the spacecraft that encounters the FTE before or after it enters the FTE or obtained from measurements made by another THEMIS spacecraft located in the sheath. The number density N_{FTE} was sampled within 12 s of the reversal point of B_N. Here only 18 T-FTEs and 14 C-FTEs were considered because of the plasma data gaps during the other events. The distributions show that in 75% of the T-FTEs, the number density ratio, $N_{FTE}/N_{MSheath}$, is <0.5, whereas inside 90% of the C-FTEs the ratio was >0. 5. These results not only evidently indicate that the number density inside a C-FTE is larger than that inside a T-FTE but also show that the number density inside an FTE has some dependence on the background sheath number density. Figure 12b displays the cumulative distributions of FTEs as functions of the ratio of the field strength in the central region of FTEs to that in the background magnetosphere ($B_{FTE}/B_{MSphere}$). B_{FTE} was taken as the field strength associated with the reversal of B_N. Inside 80% of the T-FTEs, the field strengths exceed the background magnetospheric field strength, whereas inside 95% of C-FTEs, the field strengths are weaker than the background magnetospheric field. Figure 12c plots the cumulative distributions of FTEs as functions of the velocity parallel to the magnetic field in the central region of FTEs, where the field lines are not very different with the axes of FTEs. The parallel velocities inside both types of FTEs are evenly distributed from 0 to 150 km/s since both curves have almost a constant slope. The curve for C-FTEs slightly shifted to the right suggests that inside C-FTEs the parallel velocities are stronger than those inside T-FTEs, with average parallel velocities of 73.6 km/s for C-FTEs and 57.7 km/s for T-FTEs. However, the difference is smaller than the standard error of the mean and may not be significant.

6. Discussion and Conclusions

[45] In the early stage of the THEMIS mission, all five spacecrafts were in similar orbits. The pearls-on-a-string configuration provided a unique opportunity to investigate FTE structures using multipoint measurements with appropriately distributed impact parameters. These special orbits gave numerous opportunities for satellites to go through the central region of an FTE. The data from the early orbits have enabled us to distinguish C-FTEs from T-FTEs. During the period of the study, from 1 May 1 to 31 October 2007, C-FTEs were observed much less frequently than typical ones. The different occurrence probabilities of these two kinds of events give us an important clue to the interpretation of their formation and relation.

[46] Let us first consider proposed sources of the difference in light of the data that we have obtained in this study. It has been proposed that the formation of the two types of FTEs depends on the IMF conditions, and that quasi-antiparallel reconnection generates C-FTEs in the presence of southward IMF [e.g., *Ding et al.*, 1991], and component reconnection with strong guide fields generates T-FTEs when the IMF has a significant B_Y component [*Scholer*, 1988]. Because antiparallel reconnection can occur only in limited regions of the magnetopause whereas component reconnection is always possible somewhere on the magnetopause, the proposed model of FTE formation predicts that more T-FTEs than C-FTEs should have been generated, just as we observed. However, our studies show that both the forms of FTEs occur within the clock angle

range from 50° to 180° and that T-FTEs are actually more likely to occur for larger clock angles. This finding is the opposite of what would be expected for the *Ding et al.* [1991] and *Scholer* [1988] models. Their assumption is also inconsistent with the IMF conditions of our case studies. On 30 July 2007, the IMF clock angle was ~90°, an orientation for which the model predicts that reconnection would generate a T-FTE, whereas a C-FTE was observed. On 20 May 2007, the IMF clock angle was 118°, which is larger than the C-FTE case, and for this IMF clock angle, the model would predict formation of an FTE with a weaker core field than the C-FTE. In actuality, in this event the core field was very strong and even exceeded the background magnetospheric field strength, and we confirmed that the structure was a T-FTE. Both our case studies and our statistical studies show that the IMF clock angles only control whether or not reconnection occurs but do not relate to the type of FTE. Thus, the argument that reconnection in the presence of lower (higher) shear angle provides a stronger (weaker) guide field and thus generates FTEs with stronger (weaker) core fields is not consistent with our findings.

[47] Magnetosheath beta may also play a role in the formation of a T-FTE or C-FTE. It is possible that when beta is high, more plasma can be incorporated into an FTE, and thus, in the center of the newly formed FTE, thermal pressure can partially balance the magnetic tension of the surrounding twisted fields, and there is no need of a strong core field. However, in our study we found no clear effect of ion beta in the magnetosheath on the structure of the FTEs.

[48] As neither IMF clock angle nor plasma beta control the structure of dayside FTEs, we consider the possibility that C-FTEs are an initial, short-duration phase of the evolution of T-FTEs. We were very lucky to encounter a C-FTE event on 30 July 2007 during which spacecraft recorded its evolution toward a T-FTE. During the early inbound pass of the spacecraft P2, this FTE had the characteristics of a C-FTE, with the strength of the field decreasing near the core, a form that was successfully fitted to the KK95 flux rope model. At this stage, the particles were confined well within the structure, and there was no net plasma transport along field lines. Both high- and low-energy particles coexisted, and the differential flux of the high-energy electrons (2–4 keV) enhanced in the core region 20 s after P2 entered into the FTE structure. The thermal velocity of these high-energy electrons is approximately 6 R_E/s, and if these electrons were sucked into the structure right after the formation of the structure, their path length would have been at least 120 R_E. This distance seems improbable for the length of a structure arising from reconnection at the magnetopause, so it seems more probable that these electrons of magnetospheric origin were reflected at some mirror point in the magnetosheath and bounced within the FTE structure. We have no explanation of how a mirror point would be produced within the portion of the flux rope lying in the magnetosheath. Another possible interpretation is that these particles of magnetospheric origin were sucked into the core region shortly before they are observed by reconnection possibly suddenly occurring at the end of the FTE structure. The reconnection may change of the connectivity of the field lines within the FTE structure and thus contribute to the initiation of the parallel flow. For example, initially the field lines may connect to the sheath region at both ends of the FTE [*Fu et al.*, 1990], so there is no thermal pressure gradient along field lines. Continuing reconnection at the ends of the FTE may suddenly change the connectivity of the field lines and make them link to the magnetosphere at one ends while the other ends remain linked to the sheath. Thus, a strong pressure gradient may be established along field lines and lead to parallel flows [*Ma et al.*, 1994]. Such a connectivity change would explain why the FTE structure suddenly began to evolve as the spacecraft crossed the structure. Part way through the crossing of the FTE, a strong parallel flow began and at the same time the field strength began to increase. Although we offer an interpretation of flow onset as arising in response to a change of field line connectivity, we have no global measurements to support this suggestion. Thus, it still remains an open question as to what initiates the parallel flow; further observations and models will be needed in the future to identify the actual mechanism. When B_N reversed, the field magnitude reached its maximum. This enhanced magnetic field significantly deviated from the field in the KK95 model. One could say that the C-FTE had evolved into a typical one and that the net plasma transport along the field line contributed to the evolution of the FTE.

[49] As a counterexample to the picture of an evolving flux rope, the 20 May 2007 T-FTE event was inferred to be in a steady state since both its internal and ambient fields are well fitted by an equilibrium KK95 flux rope model. Only low-energy magnetosheath-origin particles were detected inside this event, and the high-energy particles were absent. This suggests that the structure had been present for long enough for the high-energy particles to escape and magnetic reconnection had quenched, maybe long before the structure was encountered. The parallel plasma flow, which we consider as evidence of evolution of a flux rope, was also not detected within this T-FTE, a situation consistent with our conclusion that this FTE structure was no longer evolving with time.

[50] The picture of an evolving structure is also supported by our statistical studies. If a representative C-FTE is generated by magnetic reconnection, the flux tube must consist of two portions: one initially from magnetosphere, and the other one initially from the magnetosheath. Since the particle number density in the sheath, N_{MSheath}, is much larger than in the magnetosphere, plasma initially from the sheath fills the whole flux rope, including both the portion from the sheath and the portion from the magnetosphere. As the magnetospheric part of the flux tube initially contains little plasma, the number density inside an FTE should be smaller than the background sheath plasma density. Thus, one can understand that inside most of the C-FTEs the ratios $N_{\mathrm{FTE}}/N_{\mathrm{MSheath}}$ were typically smaller than 1 but greater than 0.5. As we observed in the 30 July 2007 C-FTE event, ion bulk flow along magnetic field lines could have enabled plasma to escape from the C-FTE structure. The subsequent depletion of number density (inside T-FTEs, $N_{\mathrm{FTE}}/N_{\mathrm{MSheath}}$ was below 0.5, which was smaller than that inside C-FTEs) would reduce the thermal pressure at the center of the plasma sheet and require enhanced magnetic pressure to withstand the curvature force exerted by field lines near the boundary of the FTE. That is what we found from our statistical studies. Inside almost all of the C-FTEs, which we believe to be newly formed structures, the core fields were weaker than the background magnetospheric fields ($B_{\mathrm{FTE}}/B_{\mathrm{MSphere}} < 1$),

whereas in 80% of the T-FTEs, the core fields exceeded the background geomagnetic fields with the maximum $B_{FTE}/B_{MSphere}$ up to 2.0. We believe these statistics support the model of a C-FTE evolving into a T-FTE, which can maintain its force free structure for some time. That is what we see in the quasi steady 20 May 2007 event.

[51] We noticed (Figure 12) that the parallel plasma flows in the FTEs scatter quite uniformly below 150 km/s inside the T-FTEs as well as inside the C-FTEs. The C-FTEs were evolving, while we did not detect clear parallel flow onsets in all the C-FTEs except the 30 July 2007 event. Statistically, the parallel flows within the T-FTEs are just slightly smaller than those within C-FTEs. It is possible that these T-FTEs are not in full equilibrium and that plasma flows are still transporting plasma within these T-FTE structures. It may be necessary to allow for temporal evolution when fitting an FTE structure, no matter what form it is in, C-FTE or T-FTE.

[52] Our C-FTE evolution picture is consistent with the results of an MHD simulation by *Ma et al.* [1994] in which an FTE generated by multiple X lines initially develops in the form of a C-FTE with a core field (the B_Y component) weaker in the center than near the outer boundary. Force imbalance along the axis of the flux rope accelerates and transports plasma out of the flux rope. The depletion of plasma reduces the thermal pressure and leads to a compression of the flux rope that increases the interior magnetic field strength, much as observed in the case of the 30 July 2007 event. C-FTEs and T-FTEs have counterparts in the magnetotail plasma sheet: plasmoids (with weak core fields) and flux ropes (with strong core fields). It has been suggested that a plasmoid can evolve into a flux rope [*Hesse et al.*, 1996]. When a plasmoid is initially generated by reconnection in the near-Earth tail, its extent in the cross-tail direction is much smaller than the magnetotail width. As reconnection continues, the X line extends toward both flanks of the magnetotail, and finally, the flank magnetosheath field lines contribute to the reconnection process. The change of the connectivity of the field lines within the plasmoid triggers the evolution of the plasmoid structure. Magnetic connection between the plasmoid and the magnetosheath allows particles to be accelerated by a field-aligned pressure gradient and to escape. The plasmoid cross section then shrinks and the internal field strength increases in order to remain in pressure balance after the thermal pressure collapse. Therefore, a plasmoid evolves into a flux rope with a strong core field. This temporal evolution of the core field from weak to strong within a flux rope in the tail plasma sheet has also been represented in the simulation of *Chen et al.* [2007].

[53] We found no clear difference of the locations on the magnetopause where C-FTEs and T-FTEs were found (see Figure 1). If C-FTEs are the early stage of T-FTEs, as we propose, we would expect to find them localized near their generation region. The scattered distribution of C-FTEs over a broad range of magnetic local time near the equatorial plane means that they are not preferentially generated near the subsolar point.

[54] In this paper we have argued that C-FTEs evolve into T-FTEs. We propose that parallel flows inside C-FTEs deplete the internal ion densities and reduce the thermal pressures as the central field magnitude increases to maintain pressure balance. The question then remains to account for the nature of the loss process out of the ends of the evolving C-FTEs.

[55] **Acknowledgments.** This work was supported by NASA's THEMIS project under contract NAS5-02099. Financial support for the work of the Fluxgate Magnetometer Lead Investigator Team at the Technical University of Braunschweig by the German Ministerium für Wirtschaft und Technologie and the Deutsches Zentrum für Luft- und Raumfahrt under grant 50QP0402 is acknowledged. We appreciate helpful conversations with D. G. Sibeck and C. T. Russell.

[56] Masaki Fujimoto thanks Takuma Nakamura and another reviewer for their assistance in evaluating this paper.

References

Angelopoulos, V. (2008), The THEMIS mission, *Space Sci. Rev.*, *141*, 5–34, doi:10.1007/s11214-008-9336-1.

Auster, H. U., et al. (2008), The THEMIS fluxgate magnetometer, *Space Sci. Rev.*, *141*, 235–264, doi:10.1007/s11214-008-9365-9.

Chen, L. J., et al. (2007), Observation of energetic electrons within magnetic islands, *Nature Phys.*, *4*, 19–23, doi:10.1038/nphys777.

Cowley, S. W. H. (1976), Comments on the merging of nonantiparallel magnetic fields, *J. Geophys. Res.*, *81*, 3455–3458, doi:10.1029/JA081i019p03455.

Crooker, N. U. (1979), Dayside merging and cusp geometry, *J. Geophys. Res.*, *84*, 951–959, doi:10.1029/JA084iA03p00951.

Ding, D.-Q., L.-C. Lee, and Z.-W. Ma (1991), Different FTE signatures generated by the bursty single X line reconnection and the multiple X line reconnection at the dayside magnetopause, *J. Geophys. Res.*, *96*, 57–66, doi:10.1029/90JA01989.

Dungey, J. W. (1961), Interplanetary magnetic field and the auroral zones, *Phys. Rev. Lett.*, *6*, 47–48, doi:10.1103/PhysRevLett.6.47.

Elphic, R. C., and C. T. Russell (1983), Magnetic flux ropes in the Venus ionosphere: Observations and models, *J. Geophys. Res.*, *88*, 58.

Elphic, R. C., C. T. Russell, J. A. Slavin, and L. H. Brace (1980), Observations of the dayside ionopause and ionosphere of Venus, *J. Geophys. Res.*, *85*, 7679.

Farrugia, C. J., R. P. Rijnbeek, M. A. Saunders, D. J. Southwood, D. J. Rodgers, M. F. Smith, C. P. Chaloner, D. S. Hall, P. J. Christiansen, and L. J. C. Woolliscroft (1988), A multi-instrument study of flux transfer event structure, *J. Geophys. Res.*, *93*, 14,465–14,477, doi:10.1029/JA093iA12p14465.

Gonzalez, W. D., and F. S. Mozer (1974), A quantitative model for the potential resulting from reconnection with an arbitrary interplanetary magnetic field, *J. Geophys. Res.*, *79*, 4186–4194, doi:10.1029/JA079i028p04186.

Gosling, J. T., M. F. Thomsen, S. J. Bame, R. C. Elphic, and C. T. Russell (1990), Plasma flow reversals at the dayside magnetopause and the origin of asymmetric polar cap convection, *J. Geophys. Res.*, *95*(A6), 8073–8084, doi:10.1029/JA095iA06p08073.

Haaland, S. E., et al. (2004), Four-spacecraft determination of magnetopause orientation, motion and thickness: comparison with results from single-spacecraft methods, *Ann. Geophys.*, *22*, 1347–1365.

Hasegawa, H., B. U. Sonnerup, C. J. Owen, B. Klecker, G. Paschmann, A. Balogh, and H. Reme (2006), The structure of flux transfer events recovered from Cluster data, *Ann. Geophys.*, *24*, 603–618.

Hesse, M., J. Birn, M. M. Kuznetsova, and J. Dreher (1996), A simple model of core field generation during plasmoid evolution, *J. Geophys. Res.*, *101*(A5), 10,797–10,804, doi:10.1029/95JA03149.

Kivelson, M. G., and K. K. Khurana (1995), Models of flux ropes embedded in a Harris neutral sheet: Force-free solutions in low and high beta plasmas, *J. Geophys. Res.*, *100*, 23,637–23,645, doi:10.1029/95JA01548.

LaBelle, J., R. A. Treumann, G. Haerendel, O. H. Bauer, G. Paschmann, W. Baumjohann, H. Lühr, R. R. Anderson, H. C. Koons, and R. H. Holzworth (1987), AMPTE IRM Observations of waves associated with flux transfer events in the magnetosphere, *J. Geophys. Res.*, *92*(A6), 5827–5843, doi:10.1029/JA092iA06p05827.

Lee, L. C., and Z. F. Fu (1985), A theory of magnetic flux transfer at the Earth's magnetopause, *Geophys. Res. Lett.*, *12*(2), 105–108, doi:10.1029/GL012i002p00105.

Lui, A. T. Y., D. G. Sibeck, T. Phan, V. Angelopoulos, J. McFadden, C. Carlson, D. Larson, J. Bonnell, K.-H. Glassmeier, and S. Frey (2008a), Reconstruction of a magnetic flux rope from THEMIS observations, *Geophys. Res. Lett.*, *35*, L17S05, doi:10.1029/2007GL032933.

Lui, A. T. Y., D. G. Sibeck, T. Phan, J. P. McFadden, V. Angelopoulos, and K. Glassmeier (2008b), Reconstruction of a flux transfer event based

on observations from five THEMIS satellites, *J. Geophys. Res.*, *113*, A00C01, doi:10.1029/2008JA013189.

Lundquist, S. (1950), Magnetohydrostatic field, *Ark. Fys.*, *2*, 361.

Ma, Z. W., A. Otto, and L. C. Lee (1994), Core magnetic field enhancement in single X line, multiple X line and patchy reconnection, *J. Geophys. Res.*, *99*, 6125.

McFadden, J. P., et al. (2008), The THEMIS ESA plasma instrument and in-flight calibration, *Space Sci. Rev.*, *141*, 277–302, doi:10.1007/s11214-008-9440-2.

Moldwin, M. B., and W. J. Hughes (1991), Plasmoids as magnetic flux ropes, *J. Geophys. Res.*, *96*, 14,051.

Paschmann, G., B. U. Ö. Sonnerup, I. Papamastorakis, N. Sckopke, G. Haerendel, S. J. Bame, J. R. Asbridge, J. T. Gosling, C. T. R. Russell, and R. C. Elphic (1979), Plasma acceleration at the Earth's magnetopause: Evidence for reconnection, *Nature*, *282*, 243–246, doi:10.1038/282243a0.

Paschmann, G., G. Haerendel, I. Papamastorakis, N. Sckopke, S. J. Bame, J. T. Gosling, and C. T. Russell (1982), Plasma and magnetic field characteristics of magnetic flux transfer events, *J. Geophys. Res.*, *87*(A4), 2159–2168, doi:10.1029/JA087iA04p02159.

Paschmann, G., I. Papamastorakis, W. Baumjohann, N. Sckopke, C. Carlson, B. Sonnerup, and H. Lühr (1986), The magnetopause for large magnetic shear: AMPTE/IRM observations, *J. Geophys. Res.*, *91*(A10), 11,099–11,115.

Phan, T.-D., G. Paschmann, and B. U. Ö. Sonnerup (1996), Low-latitude dayside magnetopause and boundary layer for high magnetic shear 2. Occurrence of magnetic reconnection, *J. Geophys. Res.*, *101*(A4), 7817–7828, doi:10.1029/95JA03751.

Pu, Z. Y., et al. (2007), Global view of dayside magnetic reconnection with the dusk-dawn IMF orientation: A statistical study for Double Star and Cluster data, *Geophys. Res. Lett.*, *34*, L20101, doi:10.1029/2007GL030336.

Raeder, J. (2006), Flux transfer events: 1. Generation mechanism for strong southward IMF, *Ann. Geophys.*, *24*, 381–392.

Russell, C. T., and R. C. Elphic (1978), Initial ISEE magnetometer results: Magnetopause observations, *Space Sci. Rev.*, *22*, 681–715, doi:10.1007/BF00212619.

Sanny, J., D. G. Sibeck, C. C. Venturini, and C. T. Russell (1996), A statistical study of transient events in the outer dayside magnetosphere, *J. Geophys. Res.*, *101*, 4939–4952, doi:10.1029/95JA03063.

Scholer, M. (1988), Strong core magnetic fields in magnetopause flux transfer events, *Geophys. Res. Lett.*, *15*(8), 748–751, doi:10.1029/GL015i008p00748.

Scurry, L., C. T. Russell, and J. T. Gosling (1994), A Statistical Study of Accelerated Flow Events at the Dayside Magnetopause, *J. Geophys. Res.*, *99*(A8), 14,815–14,829, doi:10.1029/94JA00793.

Shue, J.-H., et al. (1998), Magnetopause location under extreme solar wind conditions, *J. Geophys. Res.*, *103*, 17,691, doi:10.1029/98JA01103.

Sibeck, D. G., W. Baumjohann, R. C. Elphic, D. H. Fairfield, and J. F. Fennell (1989), The magnetospheric response to 8-minute period strong-amplitude upstream pressure variations, *J. Geophys. Res.*, *94*, 2505–2519, doi:10.1029/JA094iA03p02505.

Sibeck, D. G. (1990), A model for the transient magnetospheric response to sudden solar wind dynamic pressure variations, *J. Geophys. Res.*, *95*, 3755–3771, doi:10.1029/JA095iA04p03755.

Sibeck, D. G. (1992), Transient events in the outer magnetosphere-boundary waves or flux-transfer events?, *J. Geophys. Res.*, *97*, 4009–4026, doi:10.1029/91JA03017.

Sibeck, D. G., and M. F. Smith (1992), Magnetospheric plasma flows associated with boundary waves and flux transfer events, *Geophys. Res. Lett.*, *19*, 1903–1906, doi:10.1029/92GL01614.

Sibeck, D. G., M. Kuznetsova, V. Angelopoulos, K.-H. Glaßmeier, and J. P. McFadden (2008), Crater FTEs: Simulation results and THEMIS observations, *Geophys. Res. Lett.*, *35*, L17S06, doi:10.1029/2008GL033568.

Sonnerup, B. (1974), The reconnecting magnetopause, in *Magnetospheric Physics*, edited by B. M. McCormac, pp. 23, D. Reidel, Norwell, Mass.

Sonnerup, B., G. Paschmann, I. Papamastorakis, N. Sckopke, G. Haerendel, S. Bame, J. Asbridge, J. Gosling, and C. Russell (1981), Evidence for magnetic field reconnection at the Earth's magnetopause, *J. Geophys. Res.*, *86*(A12), 10,049–10,067.

Sonnerup, B., and L. J. Cahill Jr. (1967), Magnetopause structure and attitude from Explorer 12 observations, *J. Geophys. Res.*, *72*(1), 171–183.

Thomsen, M. F., J. A. Stansberry, S. J. Bame, S. A. Fuselier, and J. T. Gosling (1987), Ion and electron velocity distributions within flux transfer events, *J. Geophys. Res.*, *92*(A11), 12,127–12,136, doi:10.1029/JA092iA11p12127.

Wang, Y., et al. (2005), Initial results of high-latitude magnetopause and low-latitude flank flux transfer events from 3 years of Cluster observations, *J. Geophys. Res.*, *110*, A11221, doi:10.1029/2005JA011150.

Weimer, D. R. (2004), Correction to "Predicting interplanetary magnetic field (IMF) propagation delay times using the minimum variance technique", *J. Geophys. Res.*, *109*, A12104, doi:10.1029/2004JA010691.

Weimer, D. R., D. Ober, N. C. Maynard, W. J. Burke, M. R. Collier, D. J. McComas, N.F. Ness, and C. W. Smith (2002), Variable time delays in the propagation of the interplanetary magnetic field, *J. Geophys. Res.*, *107*(A8), 1210, doi:10.1029/2001JA009102.

Weimer, D. R., D. M. Ober, N. C. Maynard, M. R. Collier, D. J. McComas, N. F. Ness, C. W. Smith, and J. Watermann (2003), Predicting interplanetary magnetic field (IMF) propagation delay times using the minimum variance technique, *J. Geophys. Res.*, *108*(A1), 1026, doi:10.1029/2002JA009405.

Xiao, C. J., Z. Y. Pu, Z. W. Ma, S. Y. Fu, Z. Y. Huang, and Q. G. Zong (2004), Inferring of flux rope orientation with the minimum variance analysis technique, *J. Geophys. Res.*, *109*, A11218, doi:10.1029/2004JA010594.

Zhang, H., K. K. Khurana, M. G. Kivelson, V. Angelopoulos, Z. Y. Pu, Q.-G. Zong, J. Liu, and X.-Z. Zhou (2008), Modeling a force-free flux transfer event probed by multiple Time History of Events and Macroscale Interactions during Substorms (THEMIS) spacecraft, *J. Geophys. Res.*, *113*, A00C05, doi:10.1029/2008JA013451.

V. Angelopoulos, K. K. Khurana, M. G. Kivelson, R. J. Walker, J. M. Weygand, and H. Zhang, Institute of Geophysics and Planetary Physics, University of California, Los Angeles, CA 90095, USA. (hzhang@igpp.ucla.edu)

H. U. Auster and K. H. Glassmeier, Institut für Geophysik und Extraterrestrische Physik, TUBS, Mendelssohnstr. 3, D-38106 Braunschweig, Germany.

D. Larson, J. McFadden, and T. Phan, Space Sciences Laboratory, University of California, 7 Gauss Way, 7450, Berkeley, CA 94720-7450, USA.